A model for microcapsule drug release with ultrasound activated enhancement

Nadia H. Tsao and Elizabeth A. H. Hall*

Institute of Biotechnology, Department of Chemical Engineering and Biotechnology, University of Cambridge
Philippa Fawcett Drive
Cambridge, CB3 0AZ

Drug delivery; ultrasound; docetaxel; prostate cancer cells; microcapsules; microbubbles

ABSTRACT: Microbubbles and microcapsules of silane-polycaprolactone (SiPCL) have been filled with a fluorescent acridium salt (lucigenin) as a model for a drug loaded delivery vehicle. The uptake and delivery was studied and compared with similar microbubbles and microcapsules of silica/mercaptosilica (S/M/S). Positively charged lucigenin was encapsulated through an electrostatic mechanism, following a Type I Langmuir isotherm as expected, but with additional multilayer uptake that leads to much higher loading for the SiPCL system (~280 μg/2.4 × 10^9 microcapsules compared with ~135 μg/2.4 × 10^9 microcapsules for S/M/S). Whereas lucigenin release from the S/M/S bubbles and capsules loaded below the solubility limit is consistent with diffusion from a monolithic structure, the SiPCL structures show distinct release patterns; the Weibull function predicts a general trend for diffusion from normal Euclidean space at short times tending towards diffusion out of fractal spaces with increasing time. As a slow release system, the dissolution time (T_d) increases from 1 – 2 days for the S/M/S and the low concentration loaded SiPCl vehicles to ~10 days for the high loaded microcapsule. However, the T_d can be reduced on insonation to 2 days, indicating the potential to gain control over local enhanced release with ultrasound. This was tested for a docetaxel model and its effect of C4-2B prostate cancer cells, showing improved cell toxicity for concentrations below the normal EC_{50} in solution.

1. Introduction

Ultrasound has become one of the most used medical imaging methodologies in the world[1,2], since it is safe, non-invasive, low risk, portable and comparatively low cost, offers results in real-time and is relatively easy to use. However, in some cases it is limited in its application by image contrast. We have previously reported on a silica/polymer layered composite, formulated into a microbubble geometry, equivalent to the classical ultrasound contrast agent, that can be visualized and located by ultrasound as a result of the shell-gas backscatter contrast.[3] However, this silane-polycaprolactone (SiPCL) microcapsule also offers a versatile material matrix to carry active materials (e.g. drugs), since the silane derivatives can be modified and chosen to enhance or weaken interactions with the desired payload. Furthermore, as shown previously, lipase-catalyzed hydrolysis of the PCL provides a route to biodegradation and full dispersal of the spent vehicle matrix.[3] In terms of microcapsule loading, there could however, be clear disadvantages with the capacity of this geometry, since the matrix is confined to a thin layer, encapsulating the insonation-sensitive gas bubble, or dried to the inside or outside of the bubble. Nevertheless, PCL has been reported previously to be a good absorbent for polar organic compounds due to its ability to form hydrogen bonds and participate in electron donor-electron acceptor interactions.[4] In drug delivery applications, PCL has also been seen to work well in sequestering hydrophobic drugs[5,6], so that its potential as a drug carrier is clear, despite the possible limitations of a bubble geometry.

To examine the viability of a microbubble geometry to act as a payload carrier, a model compound has been chosen as a drug surrogate. The acridine nucleus[7] is found in a wide variety of drugs, offering, for example, antibacterial, antiprotozoal and antimalarial agents, but also acridine derivatives have been shown to possess activities as anti-inflammatory and anticancer agents.[8] The latter builds on the ability of the acridine chromophore to intercalate DNA and inhibit topoisomerase enzymes. Lucigenin (bis-N-methylacridinium nitrate) is a useful first model for this class of compound due to its fluorescence properties, so that encapsulation and release can be easily quantified. Lucigenin has been shown to adsorb to silica microparticles through electrostatic interactions – at neutral pH, lucigenin is positively charged while the silica microparticles have negatively charged silanols on their surfaces (the isoelectric point of silica is ~ pH 2).[9,10] This provides a convenient model for the loading of positively charged drugs. Overall, positively charged molecules have been reported to be encapsulated into silica through this electrostatic mechanism, and to follow a Type I Langmuir isotherm.[9,11–13]

One of the issues in drug administration is the balance between the delivery of a burst concentration and a sustained delivery over extended periods.[14] These challenges are now central to the drug delivery vehicle design, along with mechanisms for triggering release on demand. For example, following encapsulation, increasing the solution pH might induce the release of lucigenin through desorption[9], but there has been no information thus far on the potential for enhanced ultrasound triggered release.

The work reported herein examines the loading curves for air-filled microbubbles with and without the enzyme degradable SiPCL component, using established models, to consider the mechanism of lucigenin delivery. For comparison, delivery from microcapsules (still filled with lucigenin solution) was compared to observe the effect of microcapsule desiccation to form microbubbles, and the impact of ultrasound was considered as a potential triggering mechanism and then tested with the drug, docetaxel.

Understanding of in vitro release kinetics is a prerequisite for establishing the in vitro–in vivo relationship, to guide the formulation for performance in vivo. The loading and release of material from polymeric matrices has been studied extensively, especially in the pharmaceutical industry for the development of drug delivery vehicles. In the case of nanoparticles, many methods employ diffusion across a dialysis membrane that contains the particles[15], but for the larger microparticles, as studied here, centrifugation or filtration has been used. More importantly, modelling of the release profiles has resulted in the development of multiple empirical and semi-empirical equations. Of these, one of the most well-known is the Higuchi equation, studied for a planar vehicle releasing payload through Fickian diffusion. The simplicity of the Higuchi equation is attractive and it was modified by Baker and Lonsdale in 1974 to describe drug release from a spherical matrix, but nevertheless, more complex matrices with multilayer structure have led to increased complexity of the models as well as empirical model use.[16,17] These models form the basis for examination of payload release here.

2. Experimental

2.1 Materials

All chemicals were purchased from Sigma-Aldrich Company LLC (Dorset, UK). Cell culture media was purchased from Life Technologies (Thermo Fisher Inc., Leicestershire, UK). Cell culture plates and well plates were purchased from TTP Techno Plastics Products AG (Trasadingen, Switzerland). Cell culture microscope slides were obtained from ibidi GmbH (Martinsried, Germany). C4-2B cells were obtained from the Biorepository and Cell Services at the Cancer Research UK Cambridge Institute.

2.2 SiPCL Synthesis

The synthesis of SiPCL followed the protocol given by Tian et al.[18,19] Polycaprolactone diol (PCL diol, M_n 2000 g/mol) was end-capped with alkoxysilane groups for sol-gel functionality using 3-(trimethoxysilyl)propyl isocyanate (IPTES) and 1,4-diazobicyclo[2,2,2]octane (DABCO). The molar ratio used was 1:3:2. PCL diol and DABCO were mixed and heated to 70°C in a round bottom flask under reflux. IPTES was added to start the reaction and the reaction was carried out for 22 – 24 hours. The product, SiPCL, was collected by precipitation in methanol and filtered before drying overnight by vacuum desiccation. Successful synthesis of the SiPCL polymer was determined by Fourier-transform infrared spectroscopy (FT-IR) (Figure S.1).

2.3 Polystyrene template synthesis

The polystyrene microparticle template was fabricated using dispersion polymerization according to Lin et al.[20] Ethanol (134 mL), water (6.9 mL), styrene (50.6 mL), 4-styrene sulfonic acid (0.37 g), poly(acrylic acid) (2.26 g), and azobisisobutyronitrile (1.0 g) were mixed together in a round bottom flask under reflux at low stirring speed and degassed by bubbling with N_2. The reaction was initiated by heating to 80°C and stopped at 24 hours by cooling on ice for 5 minutes. The polystyrene was collected by centrifugation and washed with ethanol. To render the polystyrene positively charged, 0.5 w/v% polystyrene was incubated in 1 w/v% poly(allylamine hydrochloride) (PAH) solution. The excess PAH was washed off with water. The diameter of the particles, measured by transmission electron microscopy (TEM) was in a range of 2243 ± 65 nm.

2.4 Sol-gel fabrication of microcapsules and microbubbles

Microcapsules were synthesized using the modified Stöber sol-gel method as described by Lu et al.[21] and Lin et al.[20] and modified by Tsao and Hall[3]. A typical reaction consisted of the following: isopropanol (20 mL), water (3.5 mL), ammonium hydroxide (0.5 mL, 28.0-30.0% NH_3 basis), PAH-modified polystyrene (0.026 g), SiPCL (0.2 – 0.4 g) dissolved in 1 mL tetrahydrofuran (THF), and tetraethyl orthosilicate (TEOS) (0 – 214 µL). All chemicals except SiPCL and TEOS were first pre-mixed in an Erlenmeyer flask. To start the reaction, SiPCL solution was added dropwise, followed at 5 minutes by TEOS solution. The reaction was left to stir at room temperature for 5 hours, except for the 50 wt% SiPCL formulation, which was stopped at 3 hours. The reaction was terminated by removal from the solution through centrifugation. The resulting polystyrene/SiPCL/silica core/shell microparticles were washed with isopropanol, and the polystyrene was removed by incubation with THF. This resulted in a hollow SiPCL/silica microcapsule filled with THF. Vacuum desiccation could be used to remove the THF and to fill the structure with air to form microbubbles.

To make silica/mercaptosilica/silica (S/M/S) microcapsules, the ammonium hydroxide was increased to 4 mL of the 28.0 – 30.0% NH_3 basis solution. To start the sol-gel reaction, 1000 µL of TEOS was added, followed at 1 hour by 492 µL of (3-mercaptopropyl)trimethoxysilane (MPTMS) and 776 µL of TEOS at 1.5 hours. The microcapsules were collected at 3 hours and processed in the same manner as the SiPCL microcapsules.

2.5 Chemical characterization methods

FT-IR was conducted on a Perkin Elmer Spectrum One FT-IR Spectrometer (Perkin Elmer Inc., MA, USA) with an attenuated total reflectance sampling accessory attached. The spectra were read from 550 – 4000 cm^{-1}.

Imaging of microcapsules/microbubbles was conducted using TEM on a Technai G2 80-200 kV microscope (FEI, OR, USA) at 120 kV. Measurements were taken using ImageJ image processing software (National Institutes of Health, MD, USA).

Sessile drop contact angle measurements were made on approximately 8×10^7 microbubbles dried from 10 µL of microcapsule solution. A DataPhysics OCA 20 Contact Angle System (DataPhysics Instruments GmbH, Filderstadt, Germany) was used to monitor the change in 3 µL water droplets at a frame rate of 8.14 frames/second.

Dynamic light scattering (DLS) measurements were conducted on a Malvern Nano-ZS Zetasizer (Malvern Instruments Ltd., Worcestershire, UK).

2.6 Lucigenin and docetaxel encapsulation

Lucigenin was encapsulated into microcapsules by batch incubation of microcapsules in lucigenin in water solution. A stock solution of 2000 µg/mL was used. Isopropanol-filled capsules were first washed with water before encapsulation at room temperature with shaking overnight in batches of 2.4×10^9 microcapsules. The microbubbles were incubated in 1 mL of a solution of the appropriate lucigenin concentration (diluted in water). Centrifugation was used to separate out the microcapsules from the excess lucigenin solution. To form microbubbles, the microcapsules were dried under vacuum desiccation over 2 days.

Lucigenin concentration was determined by comparing the fluorescent emission of the supernatant solution to a 12-point calibration curve (0 - 3.0 µg/mL, $R^2 = 0.9977$, detection limit = 0.002 µg/mL, Figure S.2). An excitation wavelength of 370 nm was used, while emission was collected from 450 nm to 600 nm.

A 1 mg/mL docetaxel stock solution was made in ethanol. Docetaxel encapsulation was conducted in a similar manner to lucigenin encapsulation with 2.4×10^9 microcapsules. Microcapsules were washed once with ethanol before being resuspended and incubated in 1 mL of docetaxel solution overnight at room temperature with agitation.

Docetaxel concentration was determined by UV absorbance at 230 nm using a Nanodrop 1000 spectrophotometer (Thermo Fisher Scientific Inc., Leicestershire, UK). A 6-point calibration curve was made in ethanol and was found to be linear between 1 – 70 µg/mL ($R^2 = 0.9995$, detection limit = 1 µg/mL, Figure S.3).

2.7 Lucigenin delivery

To understand the release behavior of lucigenin from lucigenin-loaded microcapsules and microbubbles, the samples were tested in an open system of flowing aqueous media. Experiments were conducted in phosphate buffered saline (PBS), which closely matches physiological pH, osmolarity, and ion concentrations. The sustained delivery of lucigenin was investigated at 37°C in 0.01 M PBS. The release of lucigenin for short time (3 hours) was investigated. A separate 12-point calibration curve was made for lucigenin in PBS due to the quenching of fluorescence by chloride ions (0 – 3.0 µg/mL, $R^2 = 0.9982$, detection limit = 0.005 µg/mL, Figure S.4). The short-term sustained delivery of lucigenin was investigated using an open system which consisted of a continuous flow of fresh 0.01 M PBS at a rate of 1 mL/minute.

The release of lucigenin was tested from both 50 wt% SiPCL and S/M/S microcapsules (solution-filled) and microbubbles (air-filled) for over 180 minutes (3 hours).

A syringe filter was used as a flow cell. The lucigenin-loaded sample (2.4×10^9 microcapsules or microbubbles) was suspended in 300 µL of PBS to be loaded into the flow cell. The microcapsules and microbubbles were loaded into the flow cell prior to the start of the experiment. This was then connected to a Gilson Minipuls 2 peristaltic pump (Gilson Scientific Ltd., Bedfordshire, UK). The tubing and flow cell were immersed in a 37°C water bath throughout the experiment. The experiment was run for 3 hours. The lucigenin release recorded at very short time (circa 1 minute) included the first data before flow was started. The run-off was collected to determine the lucigenin released in each time frame. Two loading conditions were selected for the release studies – 500 µg/mL and 100 µg/mL. Only the 50 wt% SiPCL and S/M/S microbubbles were investigated. The details are presented in Table 2.

2.8 Ultrasound triggered delivery

The effect of ultrasound insonation on lucigenin delivery from microbubbles was investigated using the Terason t3000 portable ultrasound (Teratech Corporation, MA, USA). This study was confined to this portable instrument due to limitations in instrumentation that could be moved between tissue culture suites and open laboratory. A linear 12 – 5 MHz transducer (12L5) was used. The Terason Ultrasound System (Version 4.1.0) was used to control the transducer. The experiments were conducted using the same flow-cell set-up as the sustained delivery experiments. The ultrasound probe was placed in the 37°C water bath at a distance where the flow cell was in the center of the ultrasound image. Ultrasound insonation was conducted under the "high" frequency setting, which was measured to be approximately 7.3 MHz (Figure S.5) and mechanical index (MI) <0.8. Ultrasound insonation was started 30 minutes after flow of PBS was started. Samples were collected every 5 minutes for a total of 30 minutes of continuous insonation and analyzed for differences in lucigenin concentration.

2.9 Cell culture and viability

C4-2B cells were cultured in Roswell Park Memorial Institute 1640 media supplemented with 10% fetal bovine serum and L-glutamine. Cells were plated on 150 mm tissue culture plates and grown at 37°C and 5% CO_2 in a Heracell 150 incubator (Thermo Fisher Scientific Inc., Leicestershire, UK). Biocompatibility and drug delivery experiments were done in 96-well plates. Cells were plated at a density of 1500 cells/well with 90 µL media and incubated for 24 hours to allow for adhesion. Subsequently, 10 µL treatment solution was added for a total volume of 100 µL media in each well and allowed to incubate for 24 to 72 hours. The MTS assay was used to determine cell viability. Cells were incubated for 2 hours for the assay to develop and readings were taken at 490 nm. See Supporting Information for more details on the viability assay.

2.10 Incorporation of microbubbles into cells

For initial fluorescence experiments, C4-2B prostate cancer cells were plated on 100 mm dishes with 10 mL media and grown to confluency. Lucigenin-filled microbubbles were incubated with C4-2B cells at a concentration of 2×10^6 microbubbles/mL for 48 hours (a concentration of approximately 3.2×10^8 microbubbles/mL is equivalent to one dose of commercial ultrasound contrast agent). The microbubble-incubated cell samples were washed with PBS and resuspended in 10 mL media for fluorescence imaging. Incorporation was examined using brightfield and fluorescent microscopy.

For confocal experiments, approximately 20,000 cells were plated in ibidi 8-well micro- scope slides in 250 µL media. The cells were allowed to adhere over 24 hours before the microbubbles were added. Following this, the cells were stained with CellTrace Far Red dye (Life Technologies). The dye was obtained as a 50 uL aliquot and suspended in 9.9 µL DMSO. This was subsequently diluted to 5 µM in PBS. Media was aspirated and 250 µL of the dye added. This was allowed to incubate for 45 minutes at 37°C before being replaced with 250 µL cell culture media. Lucigenin-filled microbubbles were then added and allowed to incubate for 48 hours.

Images of cell culture were taken on a Nikon Eclipse TS100 microscope (Nikon UK Ltd., Kingston upon Thames, UK) with a Digital Sight DS-2Mv camera and Digital Sight DS-L2 control unit. For fluorescent images of lucigenin filled microbubbles, Nikon Intensilight C-HGFI UV source was used with a FITC filter (excitation 465 - 495 nm, dichroic mirror 505 nm, emission 515 - 555 nm).

For confocal images, a Leica TCS SP5 (Leica Microsystems UK Ltd., Milton Keynes, UK) confocal microscope with a 63×1.4 NA oil immersion lens was used. The sample was excited using an Argon laser at 485 nm and emission was collected 480 – 550 nm for the green channel and 650 – 750 for the far red channel. Image processing was done using the Fiji package of ImagesJ (National Institutes of Health, MD, USA) and Leica LAS AF Lite.

2.11 Delivery of docetaxel

Free docetaxel and docetaxel-loaded microbubbles were incubated for 72 hours in 96-well cell culture before being assessed for viability. Experiments were run with 100 nM and 10 nM maximum concentrations and were diluted 5× serially in media to 0.032 nM and 0.0032 nM respectively.

The Terason t3000 ultrasound set-up was used as described above with a focus of 2 cm. The 96-well plates were filled with media (390 µL) to acoustically couple the transducer to the sample. The plate was sealed using PCR optical adhesive film (Applied Biosystems, CA, USA). Full contact of liquid in the well with the surface of the seal was ensured. The plate was then submerged in a tank of UHP water. For insonation, the ultrasound probe was held approximately 1 cm over the wells for 30 seconds, with the bottom of the well plate and then PCR seal within ultrasound range. Figure S.6 shows a blank set-up and ultrasound insonation of microbubbles in this set up.

3. Results and Discussion

3.1 Production of lucigenin loaded microcapsules

It should be expected that the lucigenin loading of the microcapsules will depend on shell thickness and the material composition of the shell. Near-monodisperse SiPCL/silica hybrid microcapsules (polydispersity index of 0.226, measured by DLS) could be produced with shell thickness (measured from TEM micrographs) increasing from 28 to 100 nm with decreasing initial SiPCL concentration in the SiPCL/silica feed for the synthesis[3]. For comparison, the S/M/S layered microcapsules had a shell thickness of 65 ± 7 nm.

As reported previously[3], the SiPCL/silica hybrid shell behaves as if it consisted of three layers. SiPCL was added first to the polymerization feed, producing a thickness of 24 nm after 5 minutes. Subsequent addition of TEOS to the reaction mixture resulted in the condensation of silica from the more highly reactive TEOS. This dominates the reaction compared with the slower SiPCL sol-gelation, due to its smaller specific volume and lower steric crowding around the silicon atom.[22–24] The faster deposition in this phase means that the differences in shell thickness can mostly be attributed to this middle silica-rich layer which is determined by the proportion of TEOS in the reaction feed.

However, once the TEOS becomes depleted in the polymerization feed (circa 5 hours), residual SiPCL provides an outer SiPCL-rich coating on the final capsule. In contrast, early cessation of the condensation (e.g. after 3 hours) before depletion of the TEOS, yields a thinner capsule, more comparable with the S/M/S capsule; e.g. 50 wt% SiPCL, for the 3-hour synthesis microcapsules yields 77 ± 4 nm (an inner SiPCL-rich layer, ~24 nm and an outer silica-rich layer, ~53 nm) vs. 100 ± 13 nm for the 5-hour microcapsules. The 3hr capsule is missing the outer more hydrophobic SiPCL layer.

The outside surface of these capsules is therefore expected to present a more similar surface to the S/M/S capsules, but the difference in external material properties is best

demonstrated by zeta potential measurements of the microcapsules (Table 1). As can be seen in the table, for zeta potential measurements of empty microcapsules the S/M/S microcapsules produce a zeta potential that is typical for colloidal silica in the pH range 6 – 8.[25,26] In contrast, the 50 wt% SiPCL microcapsule results in a more negative zeta potential, indicative of a thicker double layer structure and a more stable colloid.

Table 1: Comparison of Zeta potential for capsules with and without lucigenin loading.

Sample	Capsule wall thickness (nm)	Zeta potential (mV)	
		Before lucigenin	After lucigenin
50 wt% SiPCL (3hr)	77±4	-71.4 ± 1.9	39.1 ± 0.1
S/M/S	65±7	-47.1 ± 2.1	-38.9 ± 0.6

Lucigenin (as a model adsorbant) has previously been shown to reach maximum sorption within 5 minutes in silica microparticles.[13] Confocal microscopy of lucigenin-loaded 50 wt% SiPCL microcapsules (3 hour synthesis) showed lucigenin in the shell structure (Figure 1a) and as can be seen in Figure 1b, at the lower loading levels for lucigenin (up to 100 µg/batch for S/M/S and 200 µg/batch for 50 wt% SiPCL microcapsules) the partition of lucigenin between solution and microcapsule had a strong preference for the microcapsules, with almost no lucigenin remaining in the supernatant after overnight incubation.

According to Zaporozhets et al.[13] lucigenin adsorbs to silica gels according to a Type I Langmuir isotherm (Equation 1).

$$V = \left(\frac{V_m K_1 C}{1+K_1 C}\right) \qquad (1)$$

where the encapsulation of lucigenin (V) is related to the equilibrium constant (K_1), the equilibrium concentration (C) after overnight incubation, and the maximum monolayer encapsulation possible (V_m). Since adsorption is limited by monolayer coverage in this model, the equation predicts a plateau in encapsulation at high solution concentrations. However, as can be seen in Figure 1b, this was not observed in the experimental data. The adsorption isotherm shows two regions with the Langmuir-like adsorption at low concentrations, whereas at higher concentrations there is a second region where lucigenin loading continues to increase approximately linearly with equilibrium solution concentration above the predicted Langmuir saturation.

The rather linear increase with equilibrium concentration could be indicative of a simple solution partitioning of lucigenin between the external solution and the solution-filled interior of the capsule. However, taking into account the void core and shell volume of the microcapsules, filled with the incubating lucigenin solution at equilibrium, this only accounts for ~20 µL/batch of 2.4×10^9 microcapsules, adding approximately 2% of the equilibrium solution (0.02 µg/batch/µg/mL) to the overall lucigenin loading.

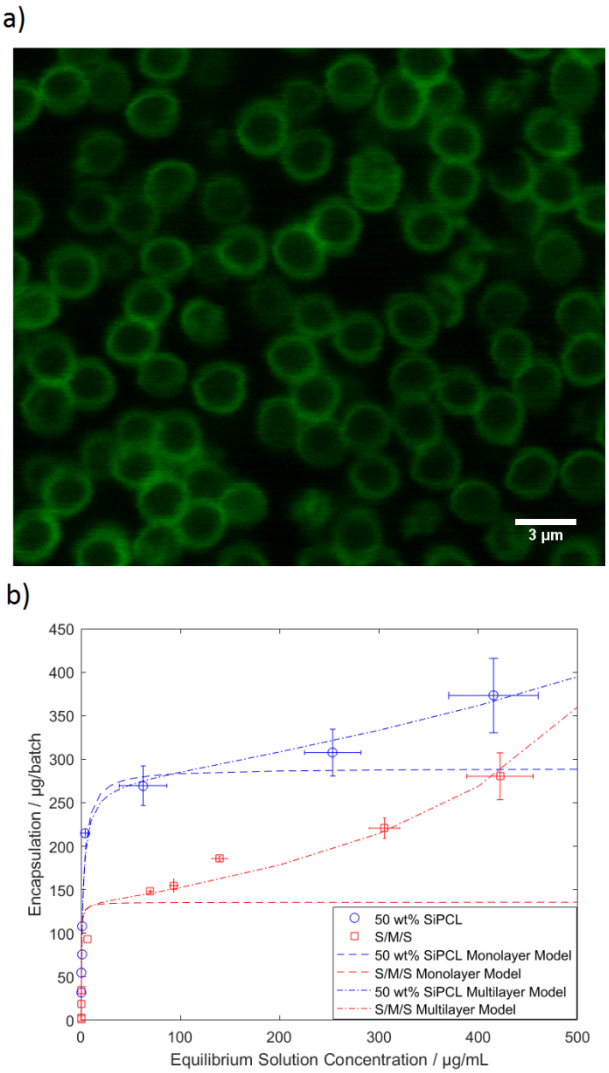

Figure 1: a) Confocal image of the lucigenin-loaded 50 wt% SiPCL microbubbles showing that the lucigenin loaded into the shell structure. b) The lucigenin loading curve. The encapsulation of lucigenin (µg/ 2.4×10^9 microcapsules) is plotted against equilibrium solution concentration after incubation overnight. Error bars represent the sum of the standard deviations of the equilibrium solution concentration and the initial loading concentration. Data is fitted to the monolayer model ($K_2 = 0$) for the lucigenin loading data and to the multilayer model.

In contrast, in the second, higher concentration region, ~35% of the amount in the equilibrium solution is being taken up for the 50 wt% SiPCL (0.345 µg/batch/µg/mL of lucigenin), whereas the S/M/S microcapsules depends on the equilibrium solution concentration (e.g. approximately 0.353 µg/batch/µg/mL of lucigenin at 200 µg/mL). This suggests a multilayer adsorption model for both capsules.

In this model, the second layer adsorbs to already adsorbed molecules. Equation 2, derived by Wang et al.[27] for dye adsorption to sludge particles, has been proposed for such a case:

$$V = \frac{V_m K_1 C}{(1-K_2 C)[1+(K_1-K_2)C]} \quad (2)$$

Equation 2 allows for the modelling of both single and multilayer adsorption where K_1 represents the equilibrium adsorption constant for the first layer (equivalent to K_1 in equation 1), and K_2 represents the equilibrium adsorption constant for the second layer. When K_2 = 0, the model assumes the form of Equation 1. As such, the approximate monolayer capacities of the microcapsules were obtained by fitting both the monolayer model (using the data in the low equilibrium solution concentration region), and the multilayer model (Figure 1b).

Both monolayer and multilayer fittings arrived at similar V_m values, with the 50 wt% SiPCL microcapsules loading significantly more lucigenin than the S/M/S microcapsules (Table 2). On the other hand, the multilayer model suggests a greater capacity for multilayer lucigenin loading for the S/M/S microcapsules (beyond monolayer saturation). These findings highlight that while the first layer of lucigenin adsorption depends greatly on the microcapsule material, overall encapsulation of lucigenin may be limited by the physical dimensions of the microcapsule such as pore volume.

Table 2: Mono- and multilayer adsorption fitting results

Sample/ Model	V_m (μg/batch)	K1 (L/μg)	K2 (L/μg)	R^2
SiPCL Mono	289.6	4.54×10^{-1}	N/A	0.97
SiPCL Multi	272.2	5.03×10^{-1}	6.25×10^{-4}	0.98
S/M/S Mono	135.6	3.24	N/A	0.95
S/M/S Multi	133.7	3.32	1.26×10^{-3}	0.98

This interpretation can also be considered in the context of the data in Table 1 which shows the increase in the zeta potential with lucigenin loading. It is noteworthy, that despite Figure 1b suggesting much higher multilayer loading for the S/M/S system, the higher monolayer adsorption and surface association of lucigenin with the 50% SiPCL (272.2 vs. 133.7 μg/batch), is reflected in the large change in zeta potential giving a strongly positive outcome.

3.2 Incorporation into cells

We have previously shown that, unlike the normal lipid based ultrasound contrast agent, microbubbles produced from these materials are exceptionally stable candidates for ultrasound contrast agents. They show a strong backscatter signal within the medically approved range of acoustic pressure[3,20] and in contrast to the lipid capsules that generally become acoustically inactive a few hours after reconstitution, they show no deterioration even after several hours, unless a degradable chemistry (such as the caprolactone) has been inbuilt.[3] Furthermore, the elasticity of the bubbles could be altered by incorporation of different organosilanes and, together with control of the bubble shell thickness, both the backscatter intensity and the ultrasound pressure required for bubble rupture could be tuned. In the case of the materials used here, no susceptibility to rupture was found for a mechanical index (MI) < 0.8.[3]

Thus, the lucigenin loaded microbubble offers an interesting model for dual function of US contrast agent and delivery vehicle. After loading with lucigenin, the microbubbles (2×10^6 microbubbles/mL loading of 200 μg lucigenin/batch) were incubated with C4-2B prostate cancer cell samples. Even after washing with PBS, a high number of microbubbles remained firmly adhered to the cells. Figure 2c and 2f shows the overlaid images indicating that the cells were healthy and properly adhered to the bottom of the dish with a clear affinity for a number of the microbubbles to associate with the C4-2B cells, especially in the case of SiPCL, where they associated in clusters. The overlay image also suggests the colocation of many of the microbubbles with the stained cytoplasm. Z-stacked images taken through the cells, is consistent with some of these microbubbles becoming incorporated into the cell as shown in Figure 2g, where the white arrow indicates one area when microbubbles have become enclosed within the cell. However, the Cell Trace Far Red dye stains primary amines in, for example, proteins, but it appears from the confocal image that the microbubbles are not in a stained compartment, which may indicate that they are not internalized in the cytosol. Internalization of large macromolecules has been reported to occur through macropinocytosis, as a non-specific event that internalizes a large volume of extracellular fluid.[28,29]

Although these data indicate some promise for the microbubbles as drug delivery vehicles, the C4-2B cell system is too complex to be able to characterize the lucigenin release profiles and draw any conclusions about the release model. In the first instance, therefore, a simple solution based model was examined to characterize the release and thence the effect of ultrasound.

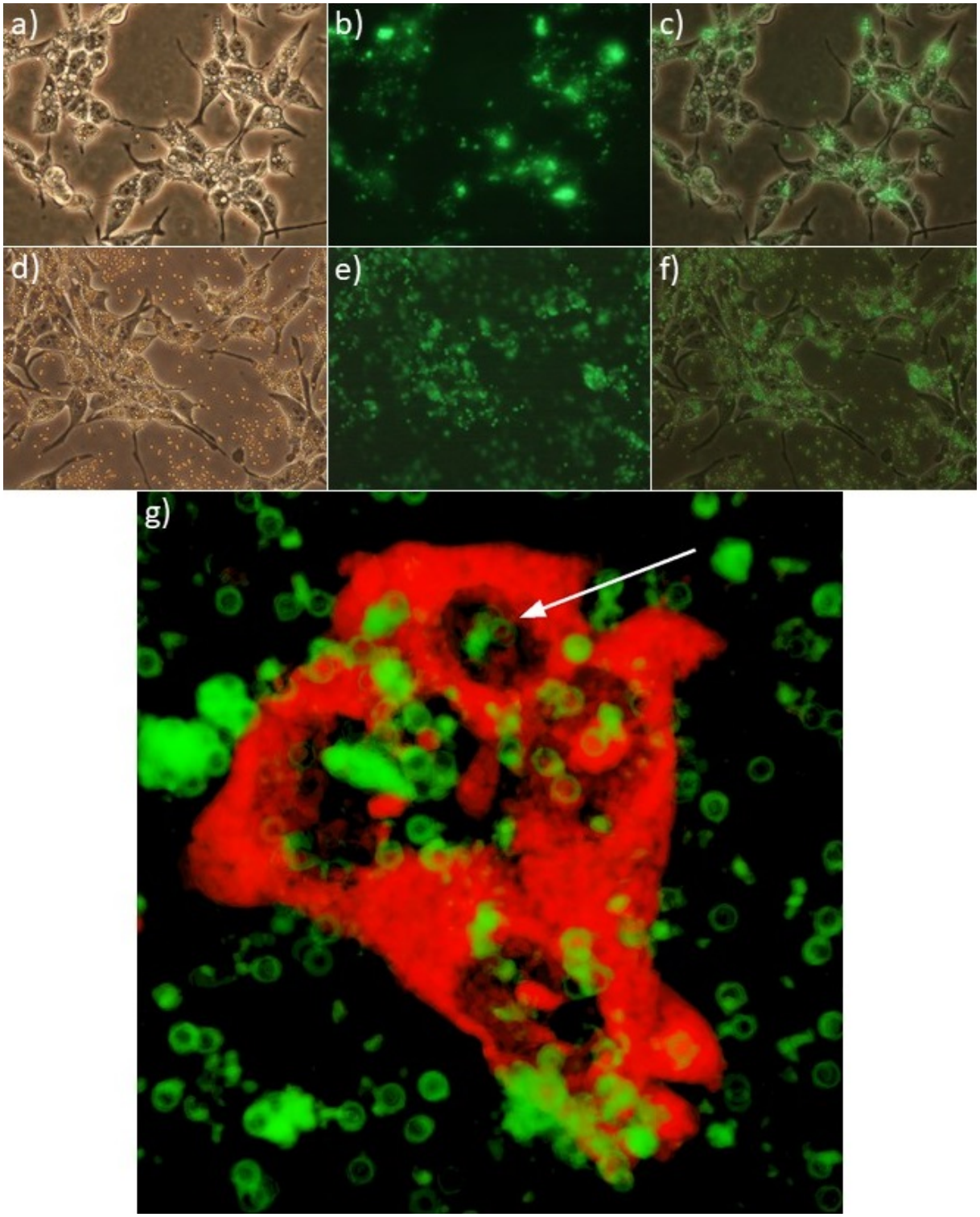

Figure 2: Microscope images of the lucigenin-filled microbubbles incubated with C4-2B prostate cancer cells showed colocation with cells. a) brightfield, b) fluorescent and c) brightfield/fluroescence overlay images of the lucigenin-filled 50 wt% SiPCL microbubbles and d) brightfield, e) fluorescent and f) brightfield/fluorescence overlay images of the S/M/S microbubbles show colocation with cells. g) 3D reconstruction of z-stacked images taken with a confocal microscope were suggestive of microbubble internalization. See Figure S.7 for z stack images.

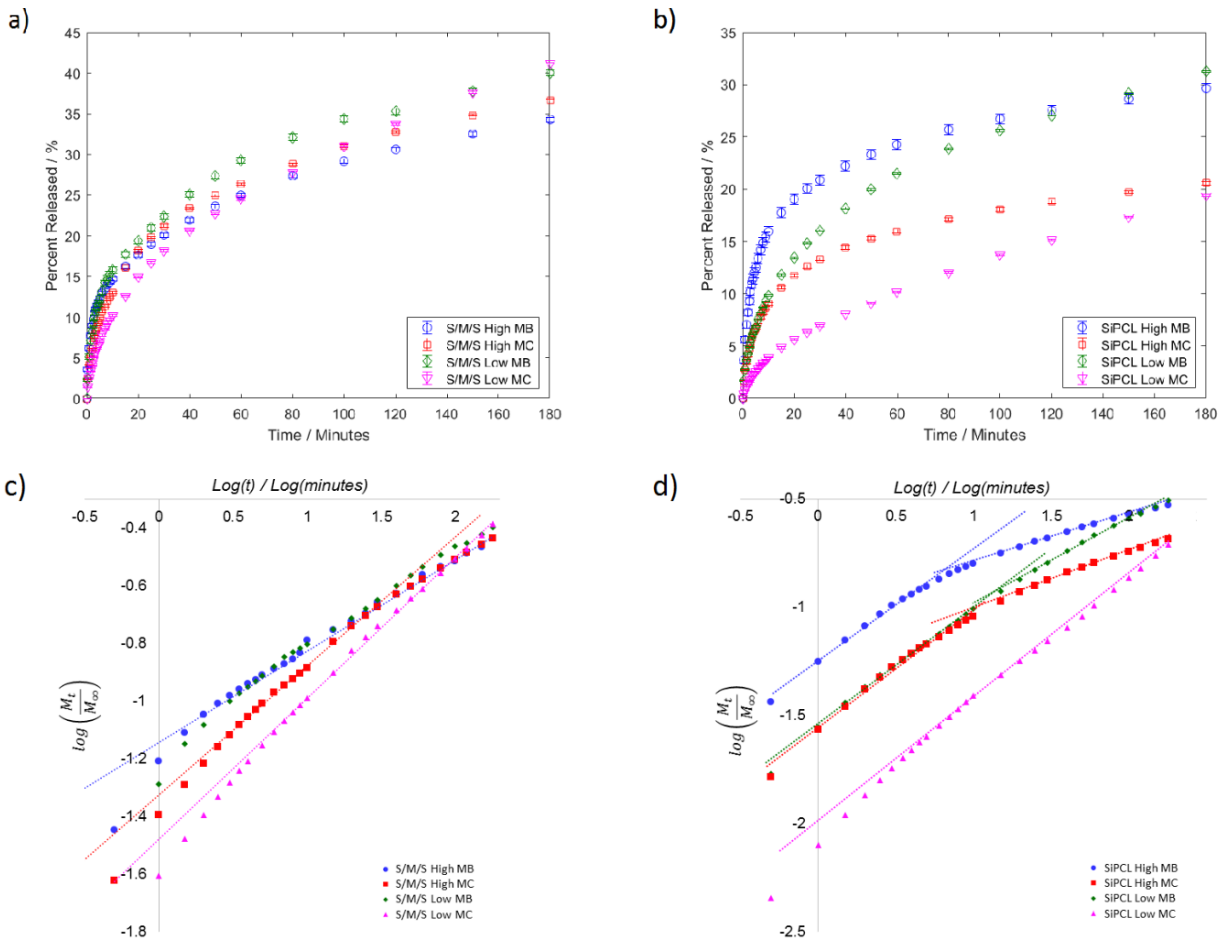

Figure 3: Release profiles of lucigenin-loaded (a) S/M/S and (b) 50 wt% SiPCL microcapsules and microbubbles. Korsmeyer-Ritger-Peppas release model of lucigenin-loaded (c) S/M/S and (d) 50 wt% SiPCL microcapsules and microbubbles of high (500 µg/mL) and low (100 µg/mL) lucigenin loading.

3.3 Delivery of lucigenin

To study the release of lucigenin from these vehicles, leaching into a background PBS solution was examined. Two loading solutions with 500 and 100 µg/mL were tested, and are referred to as "high" and "low" respectively (Table 3) and both microbubbles (with core solvent evaporated and replaced with air) and microcapsules (prior to desiccation) were examined to determine if the desiccation process affected the release profile. The slight increase in burst release from microbubbles was attributed to lucigenin redistribution during the drying process to the outside of the sample thus the higher availability resulted in a higher burst release.[30] For S/M/S samples, once the dissolution/desorption front entered the pores of the microcapsules during release, the release rate increased so that at the end of 3 hours the release from microbubbles and microcapsules were similar. However, a separate phenomenon was observed for 50 wt% SiPCL samples. The low release from microcapsules by the end of 3 hours suggested that the adsorption of lucigenin to wet SiPCL is a lot stronger than to dry SiPCL. It can be seen that delivery of lucigenin from the S/M/S bubbles and capsules is similar in all cases (Figure 3a), whereas the 50% SiPCL shows distinct characteristics for both microbubble and microcapsule as well as high and low loading (Figure 3b).

Table 3: Details of microcapsules/microbubbles tested for sustained delivery

Sample	Loading Solution (µg/mL)	Loading (µg/batch)
50 wt% SiPCL	500	259 ± 10
	100	99 ± 0
S/M/S	500	159 ± 3
	100	93 ± 0

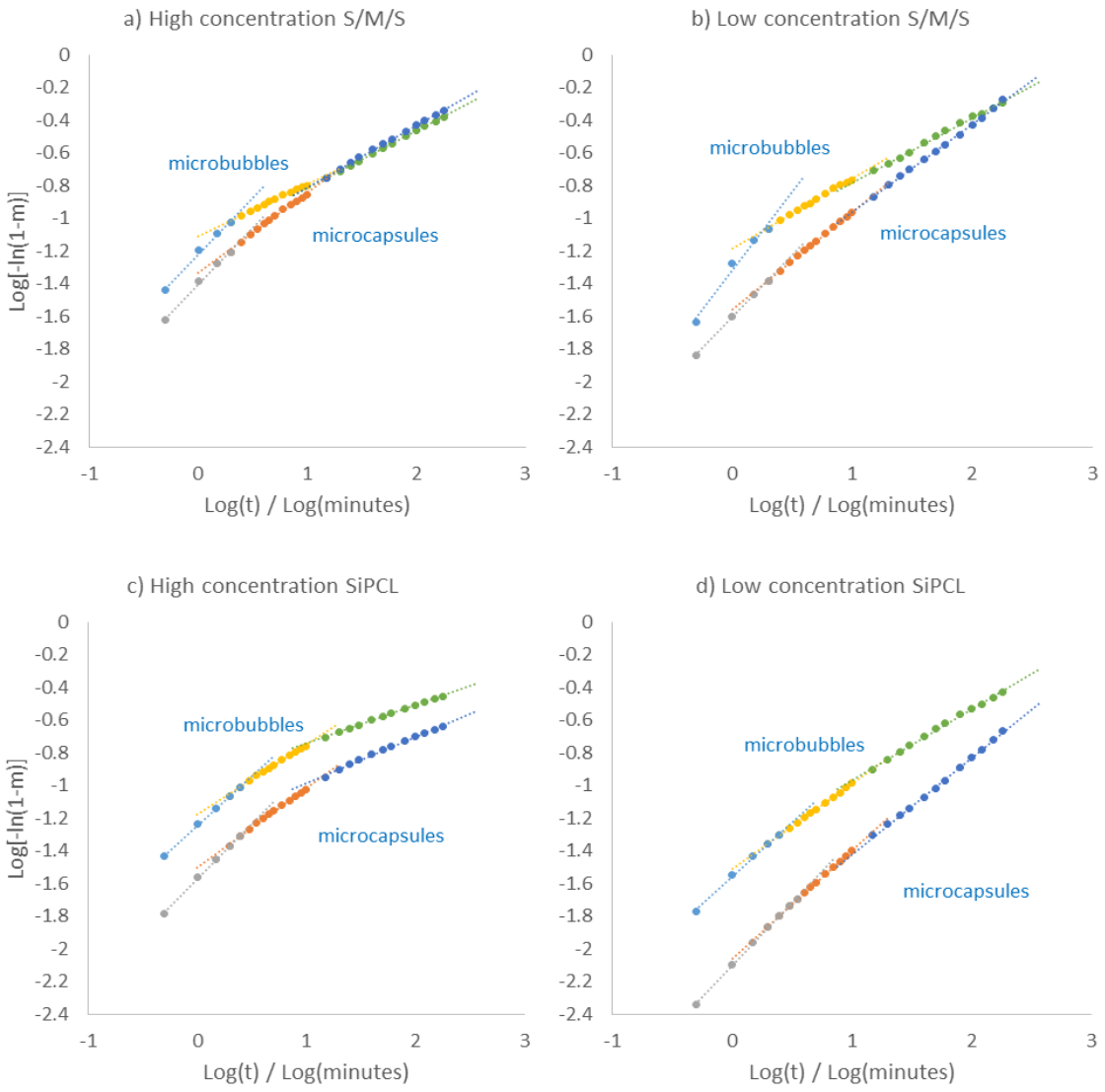

Figure 4: Log-log plots of a) high and b) low lucigenin loading of S/M/S microbubbles and microcapsules; c) high and d) low lucigenin loading of 50 wt% SiPCL microbubbles and microcapsules with associated linear fits to the regions of the Weibull equation ($m = \frac{M_t}{M_\infty}$). The data is separated out into three colors for easy visualization of the three time sections of 0 – 4 minutes, 4 – 10 minutes, and 10 – 180 minutes.

The differences between capsule and bubble for the 50% SiPCL could be due to swelling of the polymer matrix when the dry bubble is put in the aqueous environment, leading to Class II diffusion.[31] The microcapsules are dried after lucigenin loading, producing a microbubble containing an air core, whereas the microcapsules are liquid-filled. Compared with silica gel, which is hydrophilic and hygroscopic, but still well known for its non-swelling behavior after drying,[32] SiPCL is more hydrophobic, which should also point to little swelling in water, so that more Fickian than Class II diffusion would be expected to dominate.[3] If the payload release is simple diffusion with/without swelling, the Korsmeyer-Peppas/Ritger-Peppas models, which are semi-empirical diffusion based models, attempt to distinguish a diffusion release mechanism appropriate for a spherical vehicle:

$$log\left(\frac{M_t}{M_\infty}\right) = log\alpha + nlogt \qquad (3)$$

where M_t/M_∞ describes the fraction of lucigenin released at time t, α is a constant which depends on the geometric and structural properties of the system and n provides information on the release mechanism (Fickian $n \leq 0.43$ (sphere); mixed $0.85 \leq n \geq 0.43$; Case II $n \geq 0.85$).After an initial burst ($t < 4$ minutes) which is often characteristic of systems with a layer of loosely associated molecules on the outside surface[5,33,34], Figure 3c shows a reasonable linear fit for the S/M/S system at $t > 4$ minutes with n (Equation 3) in the range of 0.44 – 0.48 for the microcapsules and 0.29 – 0.33 for the microbubbles. This may be intuitive with the idea that the number of adsorption sites between lucigenin and S/M/S is relatively small (note V_g is smaller than for SiPCL, although the multilayer load is high) and the initial payload concentration is below its solubility limit and dissolves readily in solution within

the matrix, so that it presents as a monolithic solution, where the release is controlled by diffusion through the matrix.[35]

In the case of 50% SiPCL, Figure 3d shows that the data do not fit a single linear relationship. However, some features become evident from these plots. The initial release (compared at 1 minute, log(t) = 0) is higher for the microbubble than the microcapsule, inferring some rapidly removed surface dried material. The data can be fitted to a linear approximation for 4 < t < 10 minutes, with 0.55 < n < 0.59 for both bubbles and capsules, whereas for t > 10 minutes there is a clear distinction between the bubbles and the capsules (microcapsules: 0.30 > n > 0.27; microbubbles: 0.55 > n > 0.40). For low concentrations of loaded lucigenin n = 0.50 – 0.55 for t > 4 minutes; this is close to the Fickian diffusion model. This may reflect the simple monolayer adsorbate model, with concentration below the solubility limit, whereas for the multilayer (as typical in polymeric delivery vehicles) additional complexities usually occur with mixed processes of diffusion and dissolution or desorption and leaching, so that other approaches are needed to examine these data.

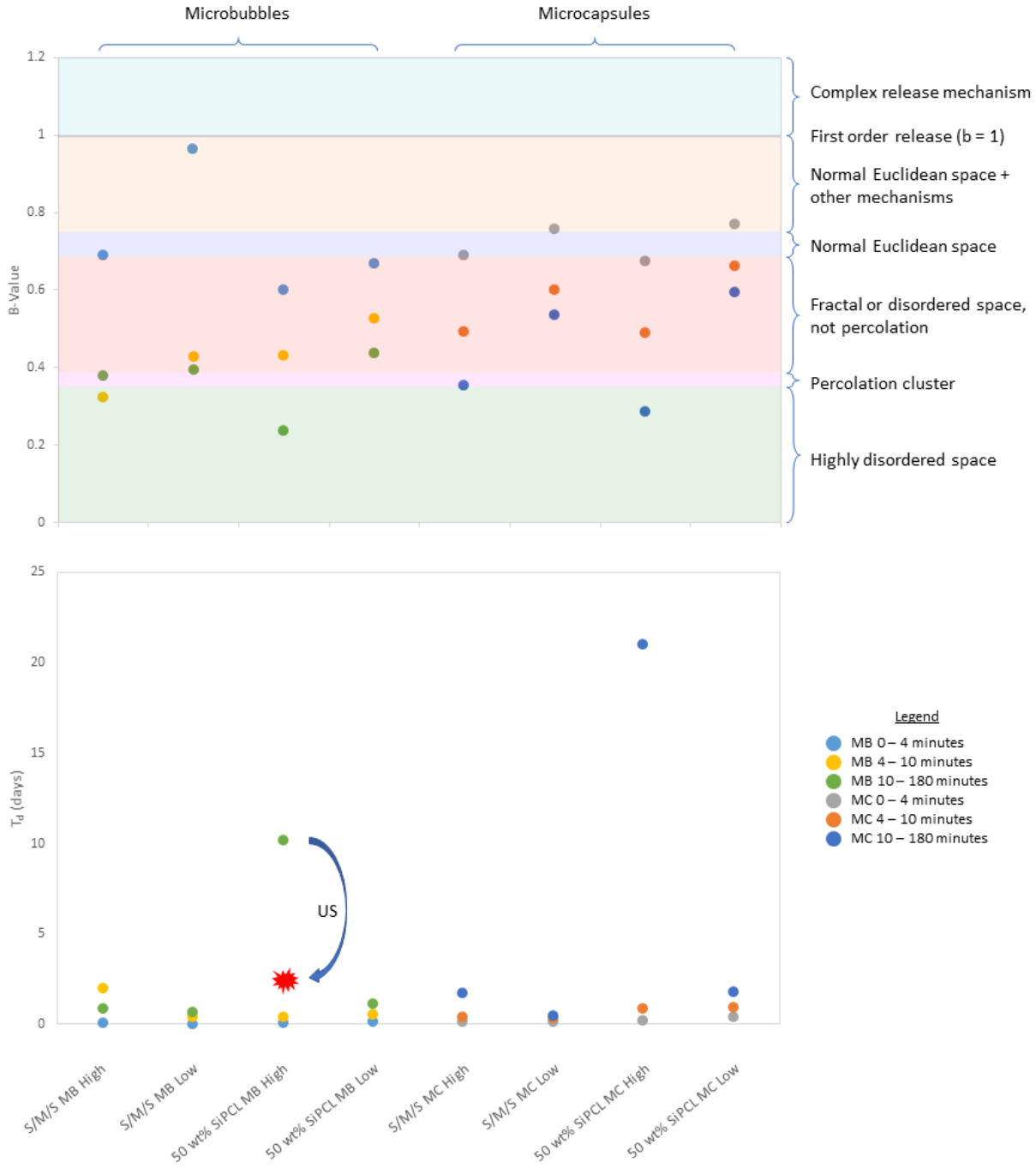

Figure 5: (a) Graph of b-values derived from Weibull model fitting for 50 wt% SiPCL and S/M/S microbubbles and microcapsules demonstrating the different regimes of lucigenin release. Release regimes as developed by Papadopoulou et al.[36] (b) From Equation 5 the 63.2% dissolution time (T_d) is given for $-\ln\left(1-\frac{M_t}{M_\infty}\right) = 1$ or $logT_{dv} = (loga)/b$.

For example, the Weibull function is a stretched exponential that has no theoretical basis but has been used extensively to examine drug dissolution and release and is able to deal with a fit to data where fractal geometry plays a role[36–38]:

$$\frac{M_t}{M_\infty} = 1 - exp\,(-at^b) \qquad (4)$$

$$log\left(-ln\left(1-\frac{M_t}{M_\infty}\right)\right) = b\,log(t) + log\,(a) \qquad (5)$$

where *a* and *b* are both constants. It has been shown that *b* can provide insight into the mechanism of diffusional release. Specifically, decreases in the value of *b* (Papadopoulou et al.[36]) have been shown to represent the slowing down of the diffusion, and has been attributed to increasing disorder of the encapsulating matrix. Durdureanu-Angheluta et al[39] have also derived a fractal "diffusion" equation which has the same form as the Weibull function where they have sought to derive the empirical constants, so that *a* and *b* are related to the fractal trajectories where $b = 2/D_F$ (D_F is the fractal dimension of the sphere).

The linearized version of the Weibull function (Equation 5) shows different linear regions (Figure 4), with slopes (*b*) that can be used to follow the trends with time attributed to the diffusion space character[36]. In this case (Figure 5a) the Weibull function generally predicts a trend for diffusion from normal Euclidean space at short times tending towards diffusion out of fractal spaces with increasing time. The microbubbles showed a greater trend to more disordered space compared with the microcapsule, which may be associated with the wetting of the pore spaces and dissolution of the lucigenin from the inner cavity surface.

In some cases, e.g. for the low concentration lucigenin loading, the two regions for t > 4 minutes are less distinct (also seen in Figure 3), consistent with the loaded lucigenin being below the solubility limit and diffusing from solution within the matrix. In this instance, the Higuchi model should provide a good fit. Higuchi used pseudo steady state assumptions to describe drug release in a matrix based on Fick's law showing a square root time dependency, which was modified by Baker and Lonsdale[40] for a spherical matrix:

$$\frac{3}{2}\left[1-\left(1-\frac{M_t}{M_\infty}\right)^{2/3}\right] - \frac{M_t}{M_\infty} = kt \qquad (6)$$

$$where\ k = \frac{3D_mC_m}{r^2C_0}$$

D_m describes the diffusion in the matrix of radius r, C_o is the starting concentration with solubility in the matrix C_m. Figure 6 plots the data according to this model and provides a reasonable fit for the S/M/S microcapsule where the payload is already in solution, below the solubility limit (Figure 6b). This plot also reveals the initial burst for the microbubble followed by a period of sustained release (t < 80 minutes) with a similar slope (k from Equation 6) to that found for the microcapsule for t < 180 minutes. This would be expected if D_m, C_m and C_o are the same in both cases, once the burst release of lucigenin from the outside of the bubble is over.

In the case of the SiPCL containing vehicles, the low concentration microcapsule data also achieves an approximate fit to this model (R^2 = 0.992), but with a noticeable upward curvature from linearity (Figure 6d). The surface hydrophobicity of these bubbles has been reported previously by us,[3] and this may be associated with the more hydrophobic characteristics, slowing the wetting and dissolution of lucigenin.

It is also clear that according to Equation 6, $k \sim 1 \times 10^{-4}$ for the S/M/S system, whereas for the SiPCL it is of lower magnitude ($k \sim 4 \times 10^{-5}$). This points to lower solubility and/or a lower diffusion in this matrix.

In contrast to the low loaded lucigenin capsules and bubbles, none of those that are loaded beyond the predicted Langmuir monolayer limit fit the Baker-Lonsdale model (Figure S.8). Looking again at the Weibull plots, it can be seen that at this loading, there is greater distinction of the three zones for the SiPCL system. For t > 30 minutes, the 50 wt% SiPCL samples enters a very slow but sustained release period, with *b* values lower than those derived in the S/M/S formulation (Figure 5a) and labelled as being from "highly disordered space". This is attributed to dissolution and diffusion of adsorbed lucigenin from the amorphous SiPCL-rich layer (a much higher V_m is seen for SiPCL than S/M/S). For these data the predicted dissolution time (T_d) reveals a distinct difference compared with the low concentration loaded SiPCL containing vehicles, with an increase in predicted T_d from 1 – 2 days for the low loaded 50% SiPCL system (and the S/M/S system for any loading) to 10 days for the high loaded SiPCL microbubble and > 20 days for the microcapsule.

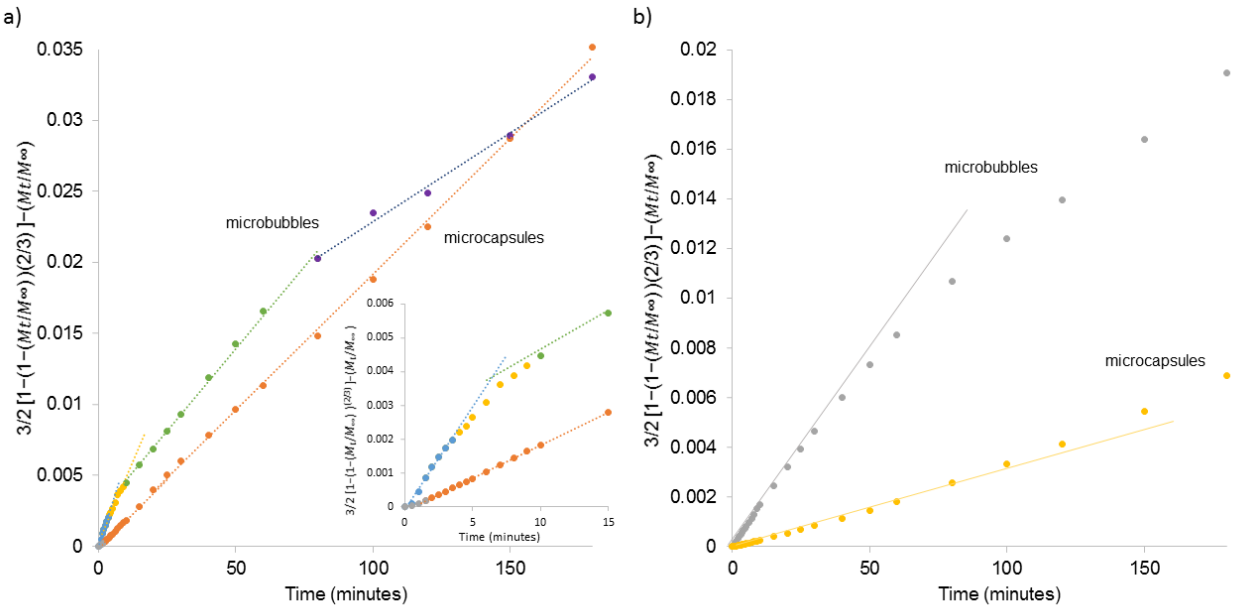

Figure 6: Baker and Lonsdale release profiles for low loading microcapsules and microbubbles of a) S/M/S and b) 50 wt% SiPCL.

3.4 Ultrasound enhanced release of lucigenin

The slow release for the 50% SiPCL after 30 minutes can be beneficial when delivery of reagent is desired over an extended period. Compared with the S/M/S model the total loading of lucigenin into this capsule is increased by > 160% so the capacity is also good. Furthermore, the microbubble offers an excellent model for examination of the effect of ultrasound on the release profile. Figure 7 compares the release profile with and without ultrasound insonation and shows that in the presence of insonation release is increased. This suggests that ultrasound could be used as a release trigger. From the Weibull function (Figure 7b), a strong change in the plot for the 50% SiPCL microbubble is evident, resulting in an increase in release rate, manifested by increase in the value of *b* towards fractal space (Figure 5). Under ultrasound control, the resultant value of T_d is reduced from 10 days to 2 days. This linear plot in this case extends the sub-30 minute trend and is nearly coincident with the data for the S/M/S system without ultrasound. The S/M/S microbubble with ultrasound also overlays these data and therefore unsurprisingly, demonstrates little change with ultrasound for this material.

The difference between the data are also found in the Baker Lonsdale plot which better separates the S/M/S data with and without ultrasound. From the slopes of the plot for 30 < t < 60 minutes ultrasound insonation increases k to ~2 × 10^{-4} and reduces the release time. According to Equation 6, this indicates that the effect of ultrasound is either improved solubility or improved diffusion.

We have shown previously that the microbubbles are able to withstand extensive insonation in the same frequency and power range as used here, without breakage.[3] Thus, the enhancement in release could have been due to microstreams generated off the surfaces of microbubbles undergoing sustained cavitation. The microstreams may have acted to promote transport of lucigenin away from the microbubble for improved desorption and dilution into the flowing PBS.[41] Additionally, it may have been possible that small oscillations of the cavitating microbubble loosened trapped lucigenin.[42–44] A third potential mechanism where ultrasound is used in release improvement is local heating due to prolonged insonation.[45] However, in the experiments undertaken here, the insonation is achieved within the limits required for low power medical ultrasound and no evidence of local heating was found.

3.5 Testing the microbubbles in C4-2B cell culture with US

Since the lucigenin did not appear to affect the growth of C4-2B cells (Figure 2), we used the findings from this model to design a docetaxel filled microcapsule. The empty microbubbles and microcapsules were found not to be toxic to the cells at concentrations below 1.0 × 10^9 microcapsules/mL (Figure S.9). This is approximately 40 times the normal ultrasound imaging concentration, and showed cell viability at 72 hours of 107.9 ± 5.7% and 109.7 ± 5.1% for the 50% SiPCL and S/M/S microcapsules respectively. This non-toxicity was not changed as a result of insonation.

For docetaxel in free solution, the threshold for cell toxicity was dependent on both time and concentration (Figure S.10) with a EC_{50} around 2 nM for 72 hours. The time effect of docetaxel was previously reported in other cell lines and has been attributed to the activation of the apoptotic pathway by the drug, through the inhibition of microtubule depolymerisation between the G_2 and M phase of the cell cycle.[46] With longer times more cells have reached the G_2/M stage and become susceptible to docetaxel toxicity. The use of US insonation did not significantly affect docetaxel toxicity.

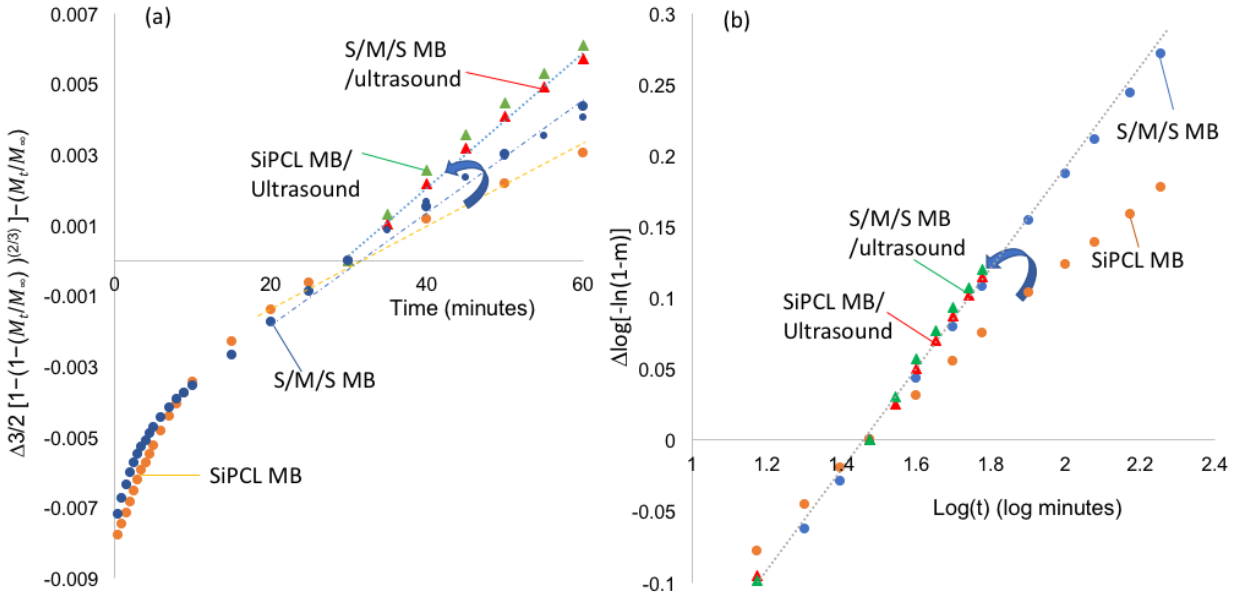

Figure 7: (a) Baker and Lonsdale and (b) Weibull release profiles for high loaded 50% SiPCL and S/M/S microbubbles before and after insonation. Ultrasound insonation was initiated 30 minutes after the start of the release of lucigenin and data is plotted with respect to the release at 30 minutes and compared with data recorded without insontation.

Following the protocol given in Section 2.11, treating the microbubbles with 200 µg/batch docetaxel solution produced a docetaxel loading of 27.0 ± 8.7 µg/batch and 36.1 ± 10.8 µg/batch for the 50% SiPCL and S/M/S microbubbles respectively. The release of docetaxel from the microcapsules and microbubbles, based on the cell viability plots (Figure 8a and b) suggest an EC_{50} equivalent of circa 10 nM (at 72 hours) in terms of the total payload concentration encapsulated in the microcapsule or microbubble. This is also indicative that total release of the docetaxel is not completed in 72 hours.

If the cell viability is observed at 2 nM total docetaxel concentration (which is around the EC_{50} for docetaxel in solution but at the threshold of the toxicity curve at 72 hours for the docetaxel loaded capsules and bubbles) then it can be seen that at 120 hours a difference emerges between the microcapsules and microbubbles (Figure S.11). Whereas the cell viability has dropped to 50% for the microcapsules (equivalent to solution administered docetaxel), it remains above 80% at this concentration for the bubbles. This follows a similar trend to the projections for lucigenin release (Section 3.3), which showed a long period of slow release at high lucigenin loadings with T_d up to 20 days for the microcapsule.

Based on these findings, it is clear that the effect of US needs to be examined at docetaxel loadings below the apparent EC_{50} for the microbubbles (i.e. < 10 nM). Preliminary results, Figure 8c and d show the effect at 72 hours, following insonation for 30 seconds. As can be seen from these data there is a clear impact even at 0.2 nM, where the microbubble in the absence of docetaxel or the free solution drug or the solution drug combined with empty microbubbles usually show any cell toxicity. This finding will require much further investigation to separate the effects due to US induced cell permeabilisation and enhanced docetaxel release from the microbubbles, but the association of the microbubbles with the cells, combined with the effect of ultrasound on both the microbubble and the cell appears to be providing a locally high effective docetaxel concentration.

4. Conclusions

This work has followed the adsorption and release of lucigenin from SiPCL and S/M/S microcapsules and microbubbles as a 'drug' model to investigate the capsules and bubbles as a drug delivery vehicle. The adsorption was seen to be able to achieve greater than monolayer coverage, depending on solution concentration. Delivery of the lucigenin from the capsules and bubbles occurs with an initial burst release, dissolving material below its solubility limit, so that it presents as a monolithic solution, where the release is controlled by diffusion through the matrix. Further delivery from the matrices shows some features of Fickian diffusion at low concentration loadings. At higher concentrations Fractal geometry appears to make an increasing impact on the release as indicated using the Weibull empirical function. The microbubbles showed a greater trend to more disordered space compared with the microcapsule, which may be associated with the wetting of the pore spaces and dissolution of the lucigenin from the inner cavity surface.

In contrast to the S/M/S systems, which showed T_d of 1 – 2 days, the 50 wt% SiPCL samples at high concentration loadings show a slow but sustained release period with a T_d of ~10 days for the microbubbles (> 20 days for the microcapsules), with *b* values indicating release from highly disordered space, attributed to the amorphous SiPCL-rich

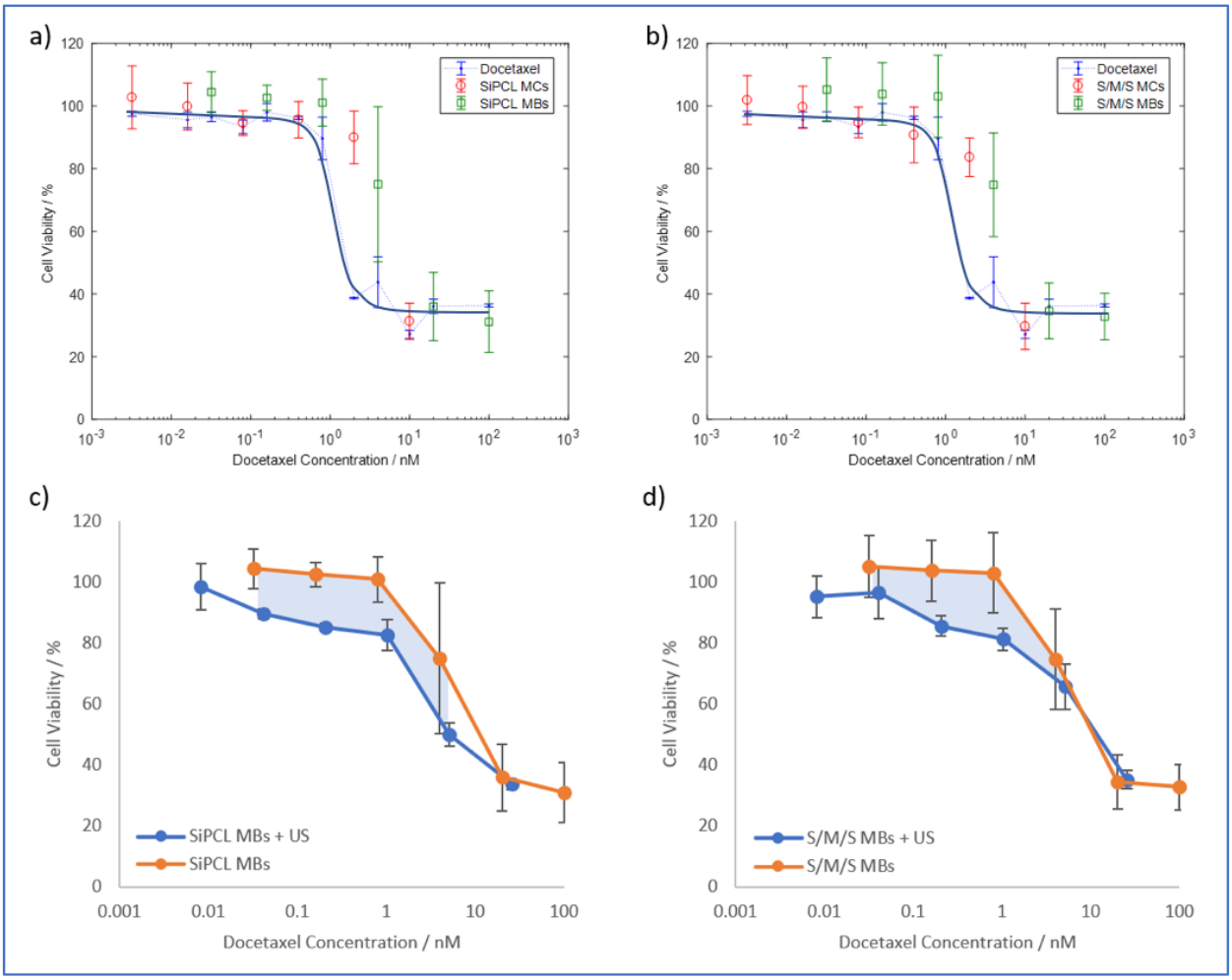

Figure 8: Cell viability of C4-2B cells showed that docetaxel released from (a) 50 wt% SiPCL and (b) S/M/S microcapsules and microbubbles was incomplete at 72 hours. Preliminary results with US insonation of (c) 50 wt% SiPCL and S/M/S microbubbles suggest enhanced delivery < 10 nM. The docetaxel concentration axis refers to the total equivalent docetaxel concentration encapsulated, not the released concentration.

layer. These data are promising for long period sustained drug release. Furthermore, these microcapsules could be triggered to increase their release rate by ultrasound insonation. Using data acquired with a standard portable medical ultrasound imaging system, the model predicted a reduction of T_d from 10 to 2 days. Based on these predictions a protocol was developed for loading the capsules and bubbles with docetaxel that were incubated with C4-2B cells. The effect of ultrasound within the medically used imaging range, on docetaxel filled microbubbles showed an increase in cell toxicity, even at concentrations below the usual solution threshold. This has potential in causing enhanced local delivery of a drug by ultrasound triggering. The mechanism for this effect, as well as the effect of various ultrasound parameters needs further investigation, but may be the result of oscillation induced dissolution of the payload or enhanced transport of the lucigenin/docetaxel from the capsule in the microstreams generated at the surface of the bubble,

ASSOCIATED CONTENT

Supporting Information. FT-IR spectra of SiPCL polymer; fluorescence calibration curve of lucigenin in water; absorbance calibration curve of docetaxel in ethanol; fluorescence calibration curve of lucigenin in 0.01 M PBS, cell viability assay; radio frequency results of microbubbles; US set up for cell culture; Baker and Lonsdale release profiles for microbubbles and microcapsules; cell viability of C4-2B cells with respect to microbubble concentration; effect of docetaxel on cells and the effect of concentration and time on cell viability; effect of time on docetaxel delivery from microbubbles and microcapsules. This material is available free of charge via the Internet at http://pubs.acs.org.

AUTHOR INFORMATION

Corresponding Author

* E-mail: lisa.hall@biotech.cam.ac.uk

Author Contributions

The manuscript was written through contributions of all authors. All authors have given approval to the final version of the manuscript.

ABBREVIATIONS

SiPCL, silane-polycaprolactone; PCL, polycaprolactone; IPTES, 3-(trimethoxysilyl)propyl isocyanate; DABCO, 1,4-diazobicyclo[2,2,2]octane; FTIR, Fourier-transform infrared spectroscopy; PAH, poly(allylamine hydrochloride); TEM, transmission electron microscopy; THF, tetrahydrofuran; TEOS, tetraethyl orthosilicate; DLS, dynamic light scattering; PBS, phosphate buffered saline; S/M/S, silica/mercaptosilica/silica; MPTMS, (3-mercaptopropyl)trimethoxysilane; MI, mechanical index.

REFERENCES

(1) Schutt, E. G.; Klein, D. H.; Mattrey, R. M.; Riess, J. G. Injectable Microbubbles as Contrast Agents for Diagnostic Ultrasound Imaging: The Key Role of Perfluorochemicals. *Angew. Chem. Int. Ed. Engl.* **2003**, *42* (28), 3218–3235.

(2) Hahn, M. A.; Singh, A. K.; Sharma, P.; Brown, S. C.; Moudgil, B. M. Nanoparticles as Contrast Agents for in-Vivo Bioimaging: Current Status and Future Perspectives. *Anal. Bioanal. Chem.* **2011**, *399* (1), 3–27.

(3) Tsao, N. H.; Hall, E. A. H. Enzyme-Degradable Hybrid Polymer/silica Microbubbles as Ultrasound Contrast Agents. *Langmuir* **2016**, *32* (25), 6534–6543.

(4) Marcinkowski, Ł.; Kloskowski, A.; Spietelun, A.; Namieśnik, J. Evaluation of Polycaprolactone as a New Sorbent Coating for Determination of Polar Organic Compounds in Water Samples Using Membrane - SPME. *Anal. Bioanal. Chem.* **2014**, *407* (4), 1205–1215.

(5) Chawla, J. S.; Amiji, M. M. Biodegradable Poly(ε-Caprolactone) Nanoparticles for Tumor-Targeted Delivery of Tamoxifen. *Int. J. Pharm.* **2002**, *249* (1–2), 127–138.

(6) Jin, M.; Piao, S.; Jin, T.; Jin, Z.; Yin, X.; Gao, Z. Improved Anti-Tumor Efficiency against Prostate Cancer by Docetaxel-Loaded PEG-PCL Micelles. *J. Huazhong Univ. Sci. Technol. Med. Sci.* **2014**, *34* (1), 66–75.

(7) Denny, W. A. Acridine Derivatives as Chemotherapeutic Agents. *Curr. Med. Chem.* **2002**, *9* (18), 1655–1665.

(8) Sondhi, S. M.; Singh, J.; Rani, R.; Gupta, P. P.; Agrawal, S. K.; Saxena, A. K. Synthesis , Anti-Inflammatory and Anticancer Activity Evaluation of Some Novel Acridine Derivatives. *Eur. J. Med. Chem.* **2010**, *45* (2), 555–563.

(9) Wu, Z.; Ahn, I.-S.; Lee, C.-H.; Kim, J.-H.; Shul, Y. G.; Lee, K. Enhancing the Organic Dye Adsorption on Porous Xerogels. *Colloids Surfaces A Physicochem. Eng. Asp.* **2004**, *240* (1–3), 157–164.

(10) Parida, S. K.; Dash, S.; Patel, S.; Mishra, B. K. Adsorption of Organic Molecules on Silica Surface. *Adv. Colloid Interface Sci.* **2006**, *121* (1–3), 77–110.

(11) Mellaerts, R.; Roeffaers, M. B. J.; Houthoofd, K.; Van Speybroeck, M.; De Cremer, G.; Jammaer, J. A. G.; Van den Mooter, G.; Augustijns, P.; Hofkens, J.; Martens, J. A. Molecular Organization of Hydrophobic Molecules and Co-Adsorbed Water in SBA-15 Ordered Mesoporous Silica Material. *Phys. Chem. Chem. Phys.* **2011**, *13* (7), 2706–2713.

(12) Radin, S.; Falaize, S.; Lee, M. H.; Ducheyne, P. In Vitro Bioactivity and Degradation Behavior of Silica Xerogels Intended as Controlled Release Materials. *Biomaterials* **2002**, *23* (15), 3113–3122.

(13) Zaporozhets, O. A.; Sukhan, V. V.; Lipkovska, N. A. Lucigenin Immobilized on Silicon Oxides as a Solid-Phase Chemiluminescent Reagent. *Analyst* **1996**, *121* (April), 501–503.

(14) Esser-Kahn, A.; Odom, S.; Sottos, N.; White, S.; Moore, J. Triggered Release from Polymer Capsules. *Macromolecules* **2011**, *44* (14), 5539–5553.

(15) Modi, S.; Anderson, B. Determination of Drug Release Kinetics from Nanoparticles: Overcoming Pitfalls of the Dynamic Dialysis Method. *Mol. Pharm.* **2013**, *10* (8), 3076–3089.

(16) Shaikh, H.; Kshirsagar, R.; Patil, S. Mathematical Models for Drug Release Characterization: A Review. *World J. Pharm. Pharm. Sci.* **2015**, *4* (4), 324–338.

(17) Lokhandwala, H.; Deshpande, A.; Deshpande, S. Kinetic Modeling and Dissolution Profiles Comparison: An Overview. *Int. J. Pharma Bio Sci.* **2013**, *4* (1), 728–737.

(18) Tian, D.; Dubois, P.; Jerome, R. A New Poly(ε-Caprolactone) Containing Hybrid Ceramer Prepared by the Sol-Gel Process. *Polymer (Guildf).* **1996**, *37* (17), 3983–3987.

(19) Tian, D.; Dubois, P.; Grandfils, C.; Jerome, R.; Viville, P.; Lazzaroni, R.; Bredas, J.-L.; Leprince, P. A Novel Biodegradable and Biocompatible Ceramer Prepared by the Sol-Gel Process. *Chem. Mater.* **1997**, *9* (4), 871–874.

(20) Lin, P.-L.; Eckersley, R. J.; Hall, E. A. H. Ultrabubble: A Laminated Ultrasound Contrast Agent with Narrow Size Range. *Adv. Mater.* **2009**, *21* (38–39), 3949–3952.

(21) Lu, Y.; McLellan, J.; Xia, Y. Synthesis and Crystallization of Hybrid Spherical Colloids Composed of Polystyrene Cores and Silica Shells. *Langmuir* **2004**, *20* (8), 3464–3470.

(22) Chen, K. C.; Tsuchiya, T.; Mackenzie, J. D. Sol-Gel Processing of Silica I. The Role of the Starting Compounds. *J. Non. Cryst. Solids* **1986**, *81*, 227–237.

(23) Radi, B. Reinforced Hydrogels for Silicone Copolymer Delivery for Scar Remediation, Queensland University of Technology, 2010.

(24) Pouxvile, J. C.; Boilot, J. P. Kinetic Simulations and Mechanisms of the Sol-Gel Polyermization. *J. Non. Cryst. Solids* **1987**, *94*, 374–386.

(25) Hu, H.; Zhou, H.; Du, J.; Wang, Z.; An, L.; Yang, H.; Li, F.; Wu, H.; Yang, S. Biocompatible Hollow Silica Microspheres as Novel Ultrasound Contrast Agents for in Vivo Imaging. *J. Mater. Chem.* **2011**, *21* (18), 6576–6583.

(26) DeMuth, P.; Hurley, M.; Wu, C.; Galanie, S.; Zachariah, M. R.; DeShong, P. Mesoscale Porous Silica as Drug Delivery Vehicles: Synthesis, Characterization, and pH-Sensitive Release Profiles. *Microporous Mesoporous Mater.* **2011**, *141* (1–3), 128–134.

(27) Wang, J.; Huang, C.; Allen, H.; Cha, D.; Kim, D. Adsorption Characteristics of Dye onto Sludge Particulates. *J. Colloid Interface Sci.* **1998**, *208* (2), 518–528.

(28) Kou, L.; Sun, J.; Zhai, Y.; He, Z. The Endocytosis and Intracellular Fate of Nanomedicines: Implication for Rational Design. *Asian J. Pharm. Sci.* **2013**, *8* (1), 1–10.

(29) Liu, J.; Kopeckova, P.; Buhler, P.; Wolf, P.; Pan, H.; Bauer, H.; Elsasser-Beile, U.; Kopecek, J. Biorecognition and Subcellular Trafficking of HPMA Copolymer-Anti-PMSA Antibody Conjugates by Prostate Cancer Cells. *Mol. Pharmacol.* **2009**, *6* (3), 959–970.

(30) Lekhal, A.; Glasser, B. J.; Khinast, J. G. Impact of Drying on the Catalyst Profile in Supported Impregnation Catalysts. *Chem. Eng. Sci.* **2001**, *56* (15), 4473–4487.

(31) Fu, Y.; Kao, W. J. Drug Release Kinetics and Transport Mechnisms of Non-Degradable and Degradable Polymeric Delivery Systems. *Expert Opin. Drug Deliv.* **2010**, *7* (4), 429–444.

(32) Park, K.; Shalaby, W. S. W.; Park, H. Introduction. In *Biodegradable Hydrogels for Drug Delivery*; Technomic Publishing Company, Inc.: Lancaster, 1993; pp 1–12.

(33) Shi, X.; Wang, Y.; Ren, L.; Zhao, N.; Gong, Y.; Wang, D.-A. Novel Mesoporous Silica-Based Antibiotic Releasing Scaffold for Bone Repair. *Acta Biomater.* **2009**, *5* (5), 1697–1707.

(34) De Koker, S.; Hoogenboom, R.; De Geest, B. G. Polymeric Multilayer Capsules for Drug Delivery. *Chem. Soc. Rev.* **2012**, *41* (7), 2867–2884.

(35) Lü, Y.; Bülow, M. Analysis of Diffusion in Hollow Geometries. *Adsorption* **2000**, *6* (2), 125–136.

(36) Papadopoulou, V.; Kosmidis, K.; Vlachou, M.; Macheras, P. On the Use of the Weibull Function for the Discernment of Drug Release Mechanisms. *Int. J. Pharm.* **2006**, *309* (1–2), 44–50.

(37) Costa, P.; Sousa Lobo, J. M. Modeling and Comparison of

Dissolution Profiles. *Eur. J. Pharm. Sci.* **2001**, *13*, 123–133.
(38) Arifin, D. Y.; Lee, L. Y.; Wang, C.-H. Mathematical Modeling and Simulation of Drug Release from Microspheres: Implications to Drug Delivery Systems. *Adv. Drug Deliv. Rev.* **2006**, *58* (12–13), 1274–1325.
(39) Durdureanu-Angheluta, A.; Bacaita, S.; Raduv, V.; Agop, M.; Ignat, L.; Uritu, C. M.; Maier, S. S.; Pinteala, M. Mathematical Modelling of the Release Profile of Anthraquinone-Derived Drugs Encapsulated on Magnetite Nanoparticles. *Rev. Roum. Chim.* **2013**, *58* (2–3), 217–221.
(40) RW, B.; Lonsdale, H. Controlled Release: Mechanism and Rates. In *Controlled release of biologically active agents*; New York, 1974; pp 15–71.
(41) Schueller, B. S.; Yang, R. T. Ultrasound Enhanced Adsorption and Desorption of Phenol on Activated Carbon and Polymeric Resin. *Ind. Eng. Chem. Res.* **2001**, *40*, 4912–4918.
(42) Coussios, C. C.; Roy, R. A. Applications of Acoustics and Cavitation to Noninvasive Therapy and Drug Delivery. *Annu. Rev. Fluid Mech.* **2008**, *40* (1), 395–420.
(43) Alzaraa, A.; Gravante, G.; Chung, W. Y.; Al-Leswas, D.; Bruno, M.; Dennison, A. R.; Lloyd, D. M. Targeted Microbubbles in the Experimental and Clinical Setting. *Am. J. Surg.* **2012**, *204* (3), 355–366.
(44) Brennen, C. E. *Cavitation and Bubble Dynamics*; Oxford University Press, 1995.
(45) Stride, E. P.; Coussios, C. C.; Wells, P. N. T. Cavitation and Contrast: The Use of Bubbles in Ultrasound Imaging and Therapy. *Proc. Inst. Mech. Eng. Part H J. Eng. Med.* **2010**, *224* (2), 171–191.
(46) Liu, C.; Zhu, Y.; Lou, W.; Nadiminty, N.; Chen, X.; Zhou, Q.; Shi, X. B.; deVere White, R. W.; Gao, A. C. Functional p53 Determines Docetaxel Sensitivity in Prostate Cancer Cells. *Prostate* **2013**, *73* (4), 418–427.

Authors are required to submit a graphic entry for the Table of Contents (TOC) that, in conjunction with the manuscript title, should give the reader a representative idea of one of the following: A key structure, reaction, equation, concept, or theorem, etc., that is discussed in the manuscript. Consult the journal's Instructions for Authors for TOC graphic specifications.

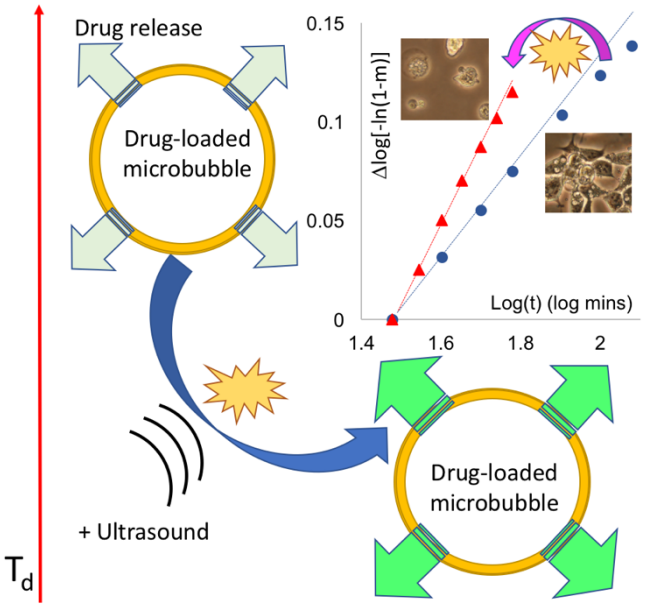

Insert Table of Contents artwork here

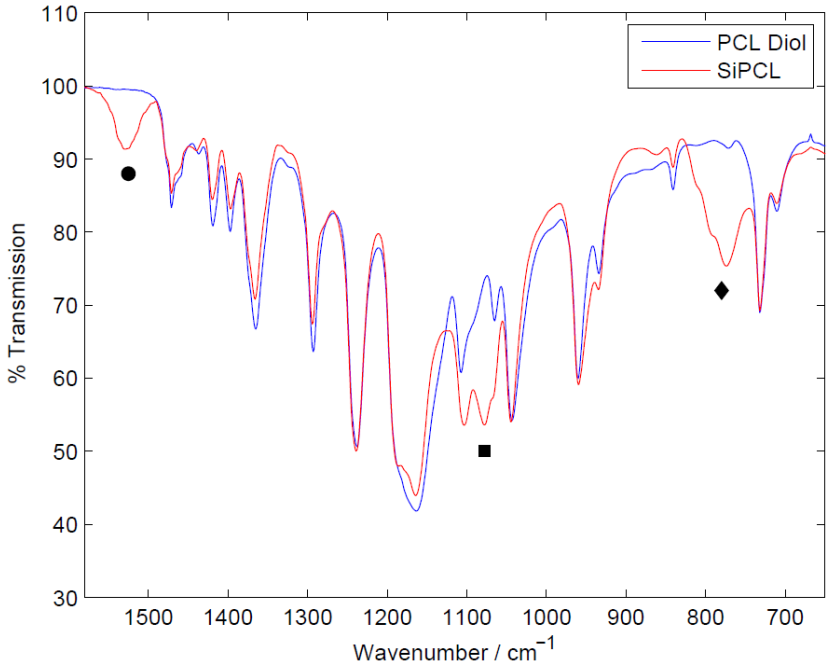

Figure S.1: FT-IR spectra of PCL diol (as supplied) and SiPCL synthesized. The SiPCL FT-IR spectra showed the appearance of an urethane linkage as determined by the N-H and C-N bend at 1525 cm^{-1} (●), and the appearance of the triethoxysilane end-cap by Si-O-C bend at 1078 cm^{-1} (■), and Si-C stretch at 780 cm^{-1} (♦).

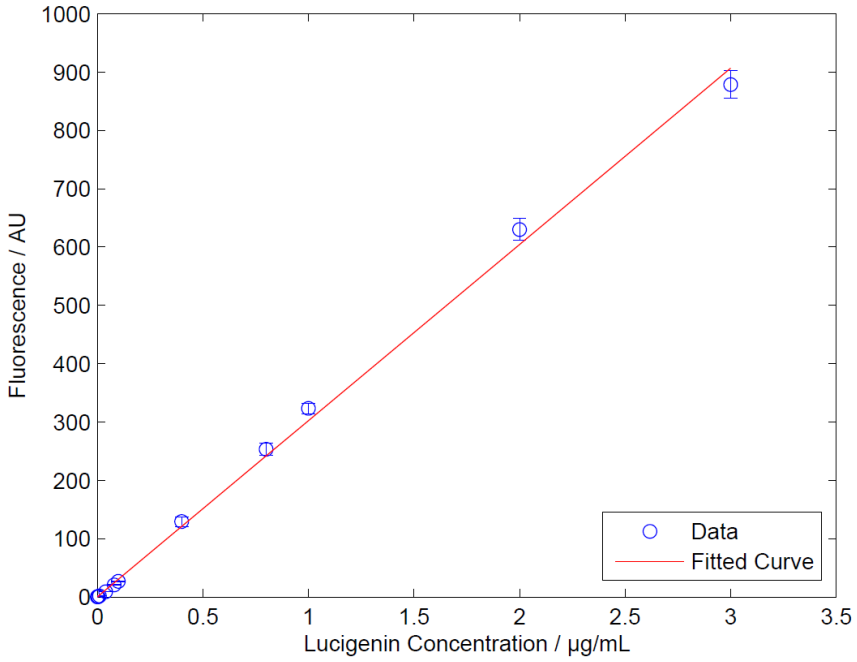

Figure S.2: Lucigenin calibration curve correlating fluorescence emission in water and lucigenin concentration.

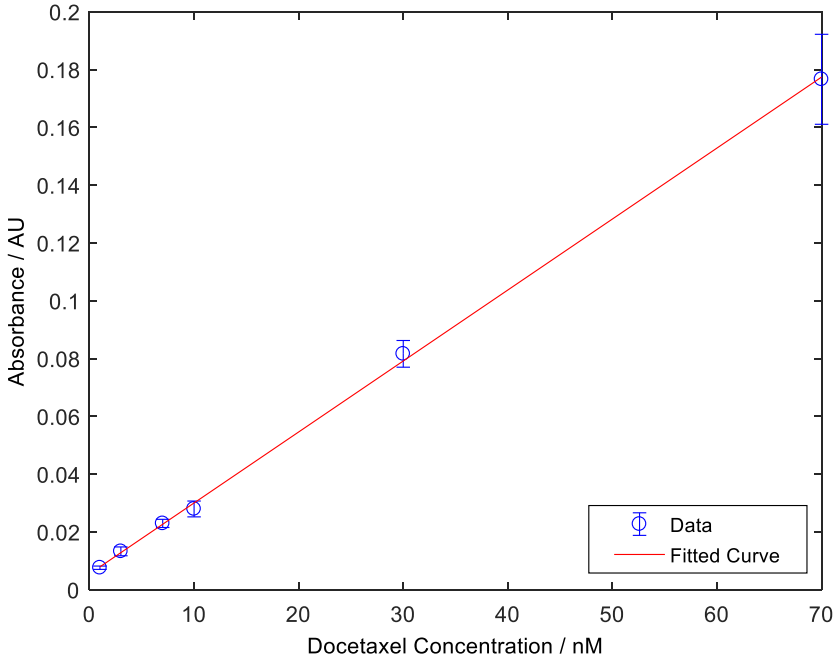

Figure S.3: Docetaxel calibration curve correlating absorbance and docetaxel concentration in ethanol.

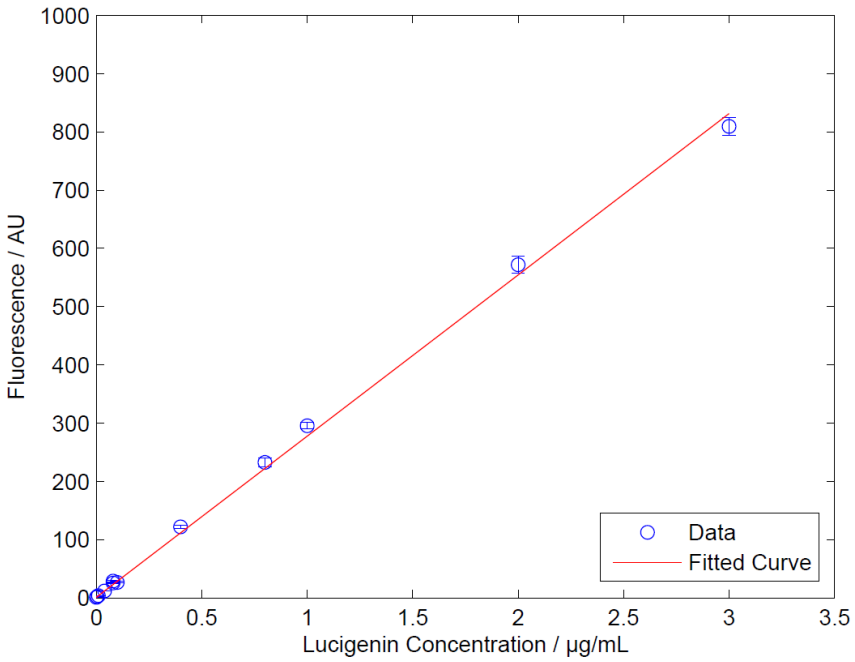

Figure S.4: Lucigenin calibration curve correlating fluorescence emission in 0.01 M PBS and lucigenin concentration.

Cell Viability Assay

Due to the high density at which the microbubbles were added to some wells, an absorbance reading at 490 nm was taken immediately prior to MTS addition. This reading served as the background from which the later MTS signal was subtracted. Following this, 20 μL of MTS was added to each well and was allowed to develop over 2 hours before the absorbance at 490 nm was taken again. The absorbance readings were taken on a Tecan Infinite M200 using i-control version 1.9 (Tecan Group Ltd., Männedorf, Switzerland), and the percent viability was calculated as follows:

$$\%viability = \frac{Abs_{post} - Abs_{pre}}{Abs_{c,post} - Abs_{c,pre}}$$

where Abs_{pre} and $Abs_{c,pre}$ are the absorbance of the sample and the control before the addition of MTS, and Abs_{post} and $Abs_{c,post}$ are the absorbance of the sample and control after 2 hours of incubation with MTS. This small correction decreased the effect of the microbubble interference of absorption at 490 nm.

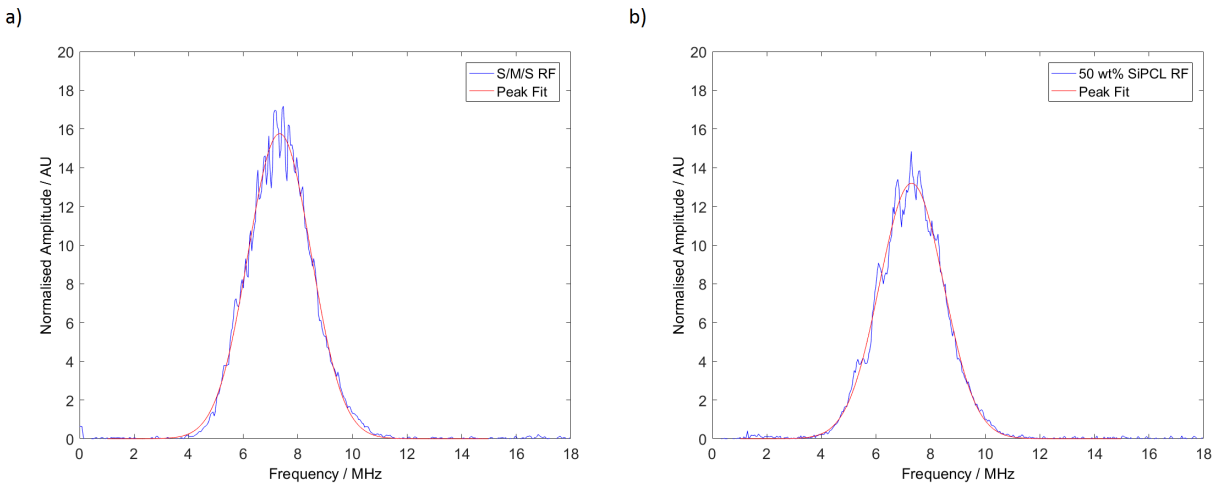

Figure S.5: Radio frequency (RF) results of the microbubbles were collected to understand the nature of the response and the frequency range of the ultrasound machine. Raw results of the microbubbles were normalized to a control of plain water. The peak fitting of the normalized RF response spectra of a) S/M/S (7.33 MHz, RMS = 0.26) and b) 50 wt% SiPCL (7.30 MHz, RMS = 0.027) microbubbles insonated with the "high" frequency setting to a single peak is shown above. No bubble rupture was observed following insonation.

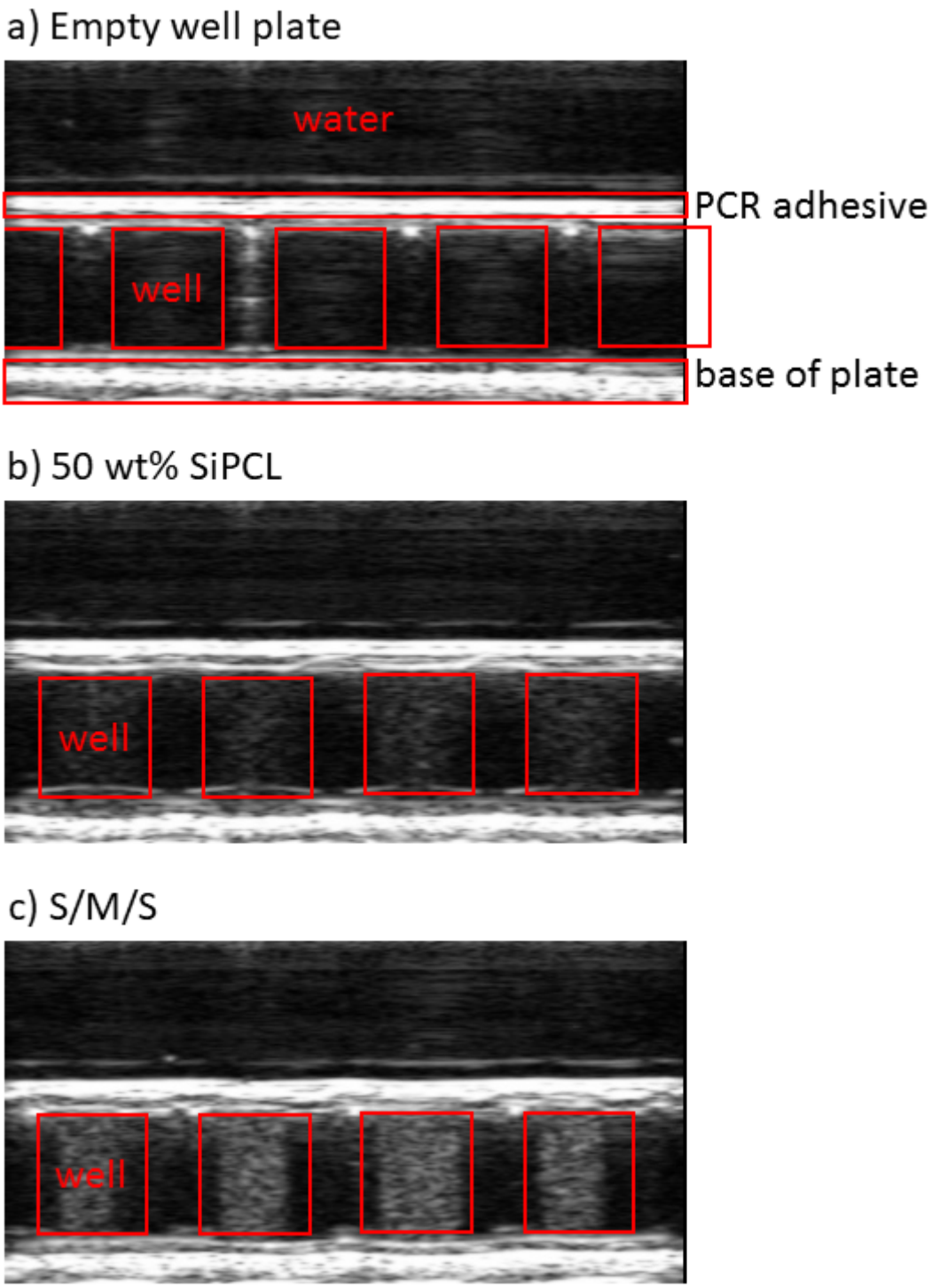

Figure S.6: Representative ultrasound image of a) blank, and 3 $\times 10^7$ microbubbles/mL of b) 50 wt% SiPCL and c) S/M/S microbubbles in the well plate set-up. The wells are outlined in red.

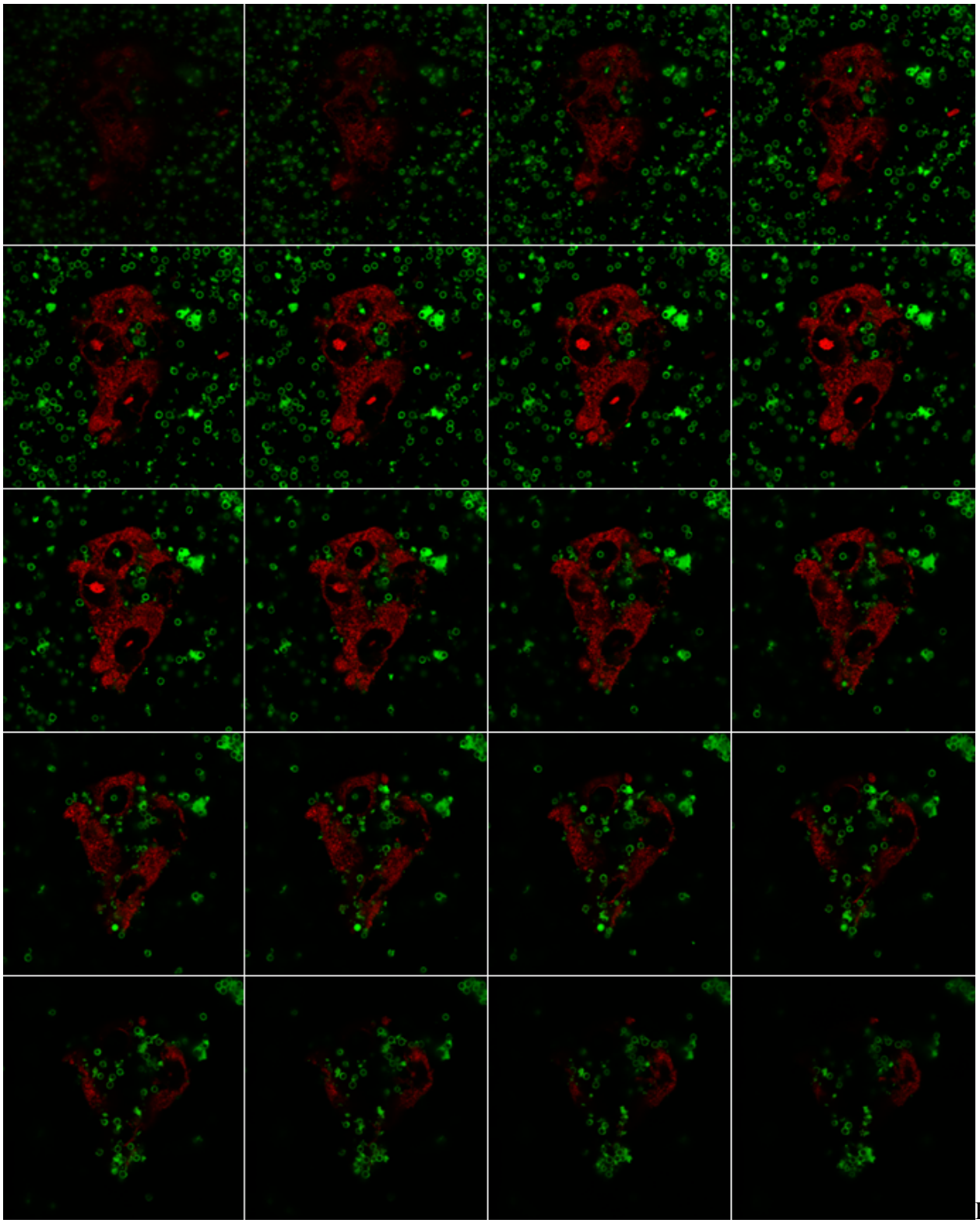

Figure S.7: Merged z-stack images of 50 wt% SiPCL microbubbles incubated with C4-2B cells were suggestive of microbubble internalization.

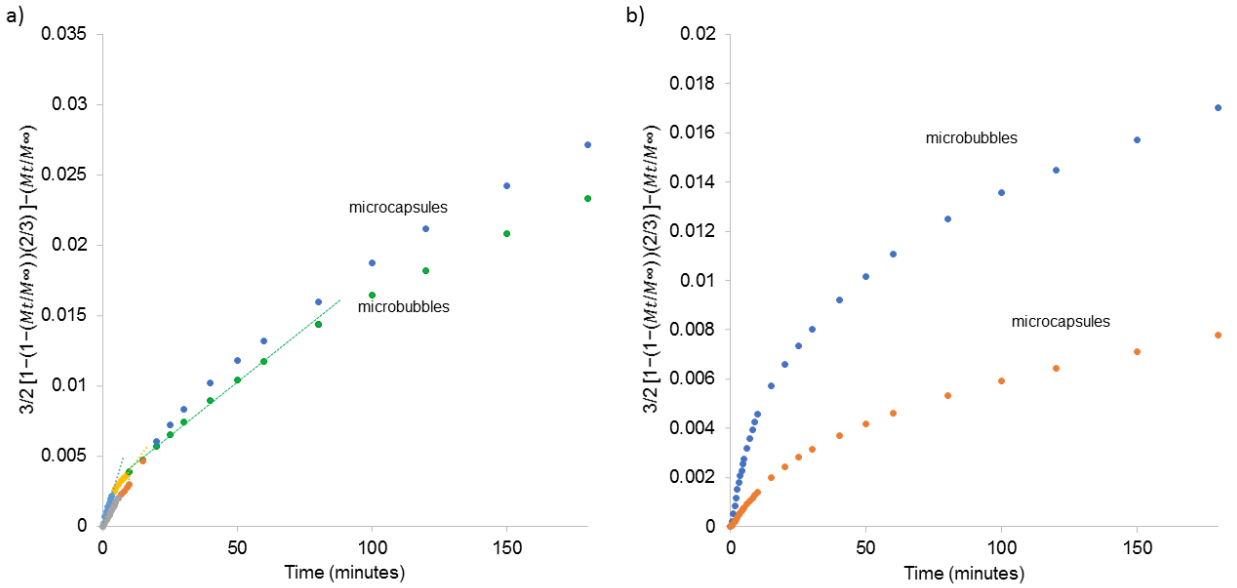

Figure S.8: Baker and Lonsdale release profiles for high loading a) S/M/S and b) 50 wt% SiPCL microbubbles and microcapsules.

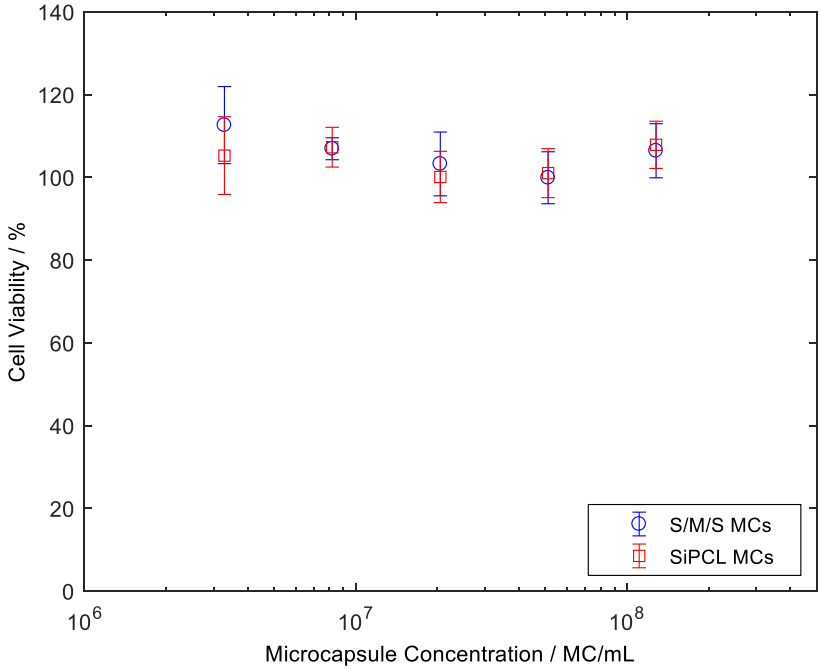

Figure S.9: Cell viability of C4-2B cells with respect to microbubble concentration after 72 hours incubation.

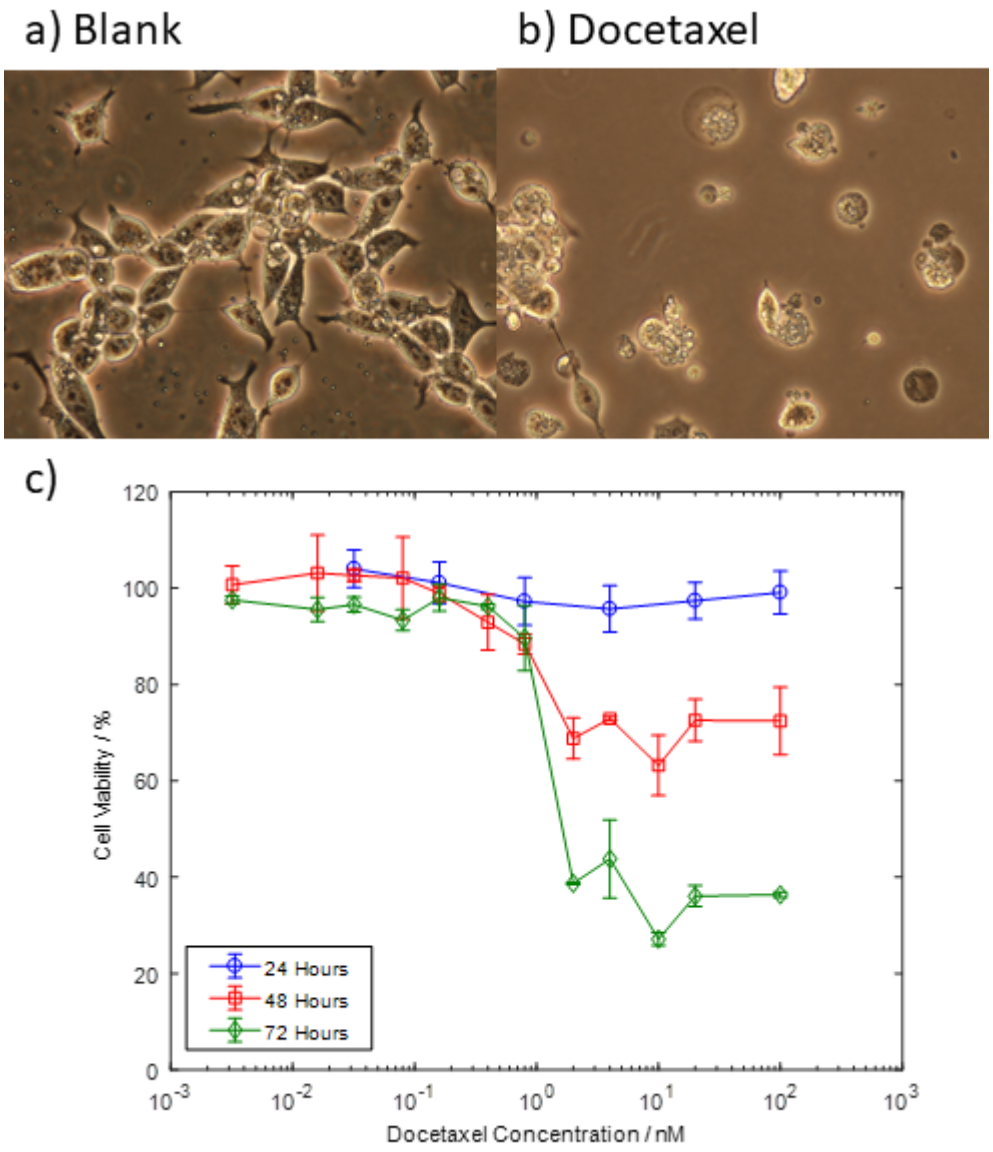

Figure S.10: Optical micrographs of C4-2B cells incubated with (a) blank and (b) docetaxel-loaded 50 wt% SiPCL microbubbles for 48 hours. Both images were taken at 400× magnification. c) demonstrates the effect of time and of docetaxel concentration on cell viability.

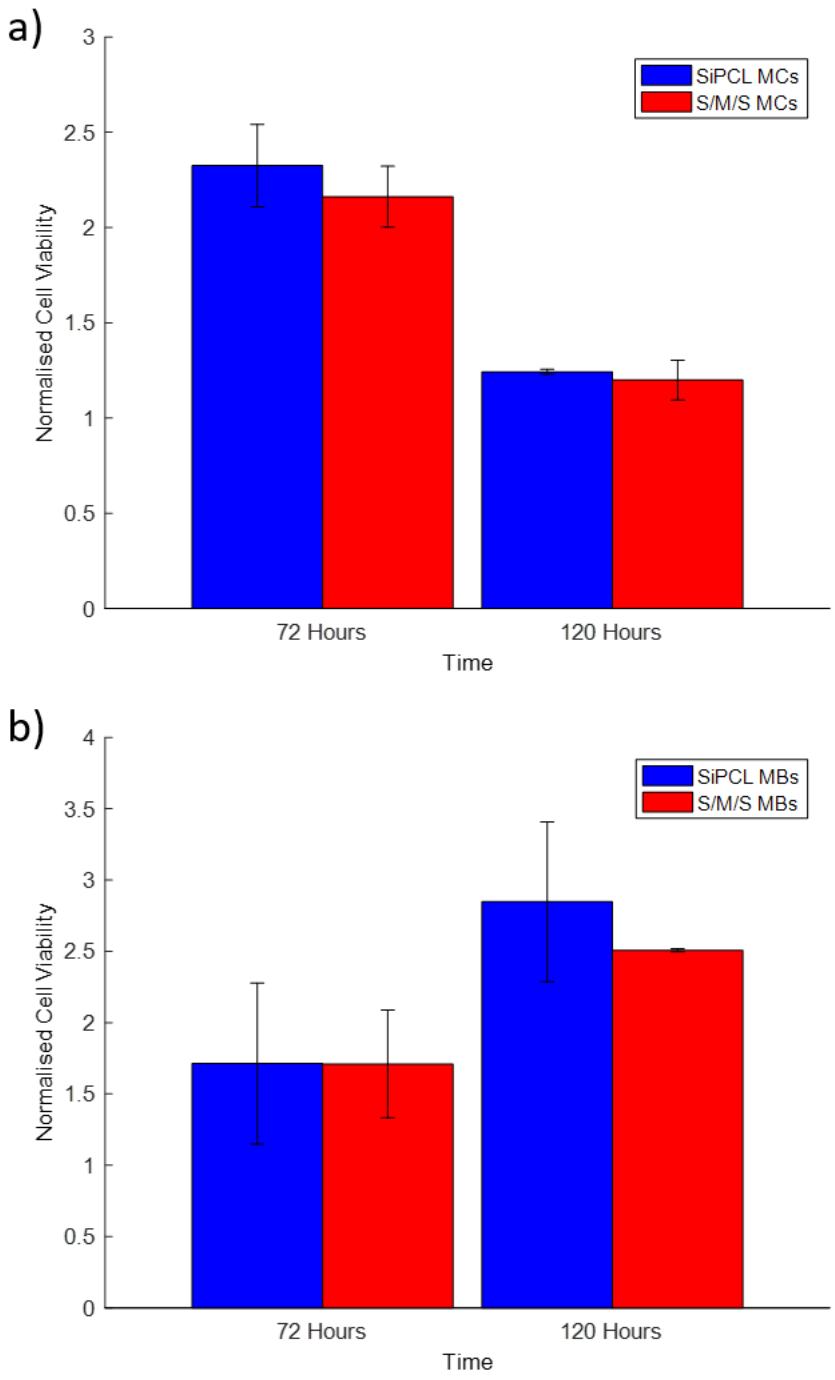

Figure S.11: Cell viability of C4-2B cells after 72 and 120 hours of incubation with a) microcapsules and b) microbubbles of 50 wt% SiPCL and S/M/S formulations, normalized to the cell viability of the same concentration of free docetaxel at those times.